Pontificia Universidad Católica del Perú

Escuela de Posgrado

Optimization of screw extrusion-based additive manufacturing process for direct extrusion of polyketone

Tesis para obtener el grado académico de Maestro en Ingeniería Mecatrónica que presenta:

Paul Jhosel Fermín Jiménez

Asesor PUCP (PUCP): *Dr. Omar Paul Troncoso Heros*

Co-Asesor TU Ilmenau: *Dr. Danka Labus Zlatanovic*

Lima, 2024

Informe de Similitud

Yo, Omar Paul Troncoso Heros, docente de la Escuela de Posgrado de la Pontificia Universidad Católica del Perú, asesor(a) de la tesis titulada(o) Optimization of screw extrusión-based additive manufacturing process for direct extrusión of polyketone, de el autor Paul Jhosel Fermín Jiménez, dejo constancia de lo siguiente:

- El mencionado documento tiene un índice de puntuación de similitud de 18%. Así lo consigna el reporte de similitud emitido por el software *Turnitin* el 27/08/2024.
- He revisado con detalle dicho reporte y la Tesis o Trabajo de investigación, y no se advierte indicios de plagio.
- Las citas a otros autores y sus respectivas referencias cumplen con las pautas académicas.

Lugar y fecha:

Lima, 27 de agosto del 2024.

<table>
<tr><td colspan="2">Apellidos y nombres del asesor / de la asesora:
Troncoso Heros, Omar Paul</td></tr>
<tr><td>DNI:
40358941</td><td rowspan="2">Firma
  </td></tr>
<tr><td>ORCID:
0000-0001-9621-2435</td></tr>
</table>

Acknowledgments

This work represents the end of a wonderful time as a student in Germany. Therefore, first I would like to thank God and my family for allowing me to live this unforgettable stage of my life.

I am deeply grateful to professor Prof. Dr.-Ing. habil. Jean Pierre Bergmann and my advisor Dr. Danka Labus Zlatanovic for guiding me during this development of my thesis and allowing me to use the laboratory equipment. Also, my thanks go to all the other colleagues from Newtonbau, technicians, researchers, etc., for supporting me all these months with my tests.

Thanks also to the professor Dr. Julio Tafur for giving me the opportunity to come to do the double degree in Ilmenau, as well as my advisor from Peru Dr. Omar Troncoso for advising me remotely.

Finally, I want to thank to all my friends and colleagues for the shared experiences during my stay in Ilmenau that helped me to continue with this thesis.

Resumen

La policetona alifática (PK) es una clase relativamente nueva de polímero semicristalino, conocida por sus propiedades químicas, térmicas y mecánicas mejoradas, así como por su respeto al medio ambiente. Estos atributos lo convierten en un candidato prometedor para reemplazar varios otros polímeros. Sin embargo, la producción de este polímero plantea un desafío debido a su limitada estabilidad térmica.

Esta tesis se centra en evaluar la viabilidad de producir piezas estables mediante fabricación aditiva basada en extrusión de tornillo para dos tipos de polecetonas alifáticas. Las policetonas utilizadas en este estudio son PK6246 (policetona base) y PK8655 (policetona reforzada con fibra de vidrio). Se empleó una metodología experimental y una caracterización detallada. Inicialmente, se realizaron pruebas preliminares para determinar y limitar parámetros como el rango de velocidad de la mesa, las dimensiones de la pieza de trabajo y las temperaturas de extrusión. Las dimensiones de la pieza de trabajo se definieron en función de las limitaciones de la mesa de impresión, mientras que el rango de velocidad de la mesa y las temperaturas de extrusión se determinaron según las recomendaciones del proveedor. Posteriormente se imprimieron 30 piezas de cada tipo de policetona.

Los resultados revelaron que se pueden producir piezas estables de PK6246 mediante fabricación aditiva basada en extrusora, cuando se eligen los parámetros de impresión correctos. Por el contrario, las piezas fabricadas con PK8655 mostraron un rendimiento deficiente. Las muestras PK6246 demostraron que las resistencias a la tracción entre capas (ángulo de impresión de 90°) pueden alcanzar valores de hasta 42 MPa, un valor razonablemente confiable considerando un ángulo de impresión de 90° y cercano a los 60 MPa especificados por el proveedor. Sin embargo, las muestras de PK8655 apenas excedieron los 30 MPa, significativamente más bajo que el valor especificado por el proveedor de 130 MPa. Además, la microestructura de las muestras de PK8655 mostró una porosidad significativamente mayor en comparación con cualquier muestra de PK6246. Además, la temperatura entre capas jugó un papel crucial en la determinación de los parámetros de impresión óptimos. Esto afecta la resistencia a la tracción y está influenciado por la velocidad de enfriamiento entre las capas, que a su vez depende de la velocidad de la mesa y la geometría de la capa. Una temperatura entre capas alta puede hacer que la pieza se hunda debido a la acumulación de calor, mientras que una temperatura entre capas baja puede provocar deformaciones, especialmente en las capas iniciales de la impresión.

Abstract

Aliphatic polyketone (PK) is a relatively new class of semicrystalline polymer, known for its enhanced chemical, thermal, and mechanical properties, as well as its environmental friendliness. These attributes make it a promising candidate to replace several other polymers. However, the production of this polymer is challenging by its limited thermal stability.

This thesis focuses on assessing the feasibility of producing stable parts through screw extrusion-based additive manufacturing for two types of aliphatic polyketones. The polyketones used in this study are PK6246 (base polyketone) and PK8655 (glass fiber-reinforced polyketone). An experimental methodology and detailed characterization were employed. Initially, preliminary tests were conducted to determine and constrain parameters such as table speed range, workpiece dimensions, and extrusion temperatures. The workpiece dimensions were defined based on printing table limitations, while the table speed range and extrusion temperatures were determined according to supplier recommendations. Subsequently, 30 pieces of each type of polyketone were printed.

The results revealed that stable parts of PK6246 can be produced through extruder-based additive manufacturing, when the correct printing parameters are chosen. In contrast, parts made from PK8655 exhibited poor performance. PK6246 samples demonstrated inter-road tensile strengths (raster angle 90°) can reach values up to 42 MPa, a reasonably reliable value considering a raster angle of 90° and close to the 60 MPa specified by the supplier. However, PK8655 samples barely exceeded 30 MPa, significantly lower than the supplier-specified value of 130 MPa. Additionally, the microstructure of the PK8655 samples showed significantly higher porosity compared to any PK6246 sample. Furthermore, the interpass temperature played a crucial role in determining the optimal printing parameters. This affects tensile strength and is influenced by the cooling rate between strands, which in turn depends on the table speed and strand geometry. A high interpass temperature can cause the piece to sink due to heat accumulation, while a low interpass temperature can lead to warping, especially on the initial strands of printing.

Zusammenfassung

Aliphatische Polyketone (PK) ist eine relativ neue Klasse teilkristalliner Polymere, die für ihre verbesserten chemischen, thermischen und mechanischen Eigenschaften sowie ihre Umweltfreundlichkeit bekannt sind. Diese Eigenschaften machen sie zu einem vielversprechenden Kandidaten für den Ersatz mehrerer anderer Polymere. Die Herstellung dieses Polymers ist jedoch aufgrund seiner begrenzten thermischen Stabilität eine Herausforderung.

Der Schwerpunkt dieser Arbeit liegt auf der Bewertung der Machbarkeit der Herstellung stabiler Teile durch additive Fertigung auf Basis der Schneckenextrusion für zwei Arten aliphatischer Polyketone. Die in dieser Studie verwendeten Polyketone sind PK6246 (Basispolyketon) und PK8655 (glasfaserverstärktes Polyketon). Es wurden eine experimentelle Methodik und eine detaillierte Charakterisierung verwendet. Zunächst wurden Vorversuche durchgeführt, um Parameter wie Plattformgeschwindigkeitsbereich, Werkstückabmessungen und Extrusionstemperaturen zu bestimmen und einzuschränken. Die Abmessungen der Werkstücke wurden auf der Grundlage der Einschränkungen der Druckplattform definiert, während der Geschwindigkeitsbereich der Plattform und die Extrusionstemperaturen auf der Grundlage der Empfehlungen des Lieferanten bestimmt wurden. Anschließend wurden 30 Stück jedes Polyketontyps gedruckt.

Die Ergebnisse zeigten, dass sich durch Extruder basierte additive Fertigung stabile Teile aus PK6246 herstellen lassen, wenn die richtigen Druckparameter gewählt werden. Im Gegensatz dazu zeigten Teile aus PK8655 eine schlechte Leistung. PK6246-Proben wiesen eine Zugfestigkeit zwischen den Schichten (Rasterwinkel 90°) auf, die Werte von bis zu 42 MPa erreichen kann, ein einigermaßen zuverlässiger Wert in Anbetracht eines Rasterwinkels von 90° und nahe an den vom Lieferanten angegebenen 60 MPa. PK8655-Proben überstiegen jedoch kaum 30 MPa und lag damit deutlich unter dem vom Lieferanten angegebenen Wert von 130 MPa. Darüber hinaus zeigte die Mikrostruktur der PK8655-Proben eine deutlich höhere Porosität als jede PK6246-Probe. Darüber hinaus spielte die Zwischenlagentemperatur eine entscheidende Rolle bei der Bestimmung der optimalen Druckparameter. Diese wirkt sich auf die Zugfestigkeit aus und wird von der Abkühlrate zwischen den Strängen beeinflusst, die wiederum von der Plattformgeschwindigkeit und der Stranggeometrie abhängt. Eine hohe Zwischenlagentemperatur kann dazu führen, dass das Teil aufgrund von Hitzestau absinkt, während eine niedrige Zwischenlagentemperatur insbesondere bei den ersten Druckschichten zu Verformungen führen kann.

Table of contents

List of figures

List of tables

List of symbols and abbreviations

A_{strand}	Area of strand
ABS	Acrylonitrile butadiene styrene
AM	Additive manufacturing
b	Strand width
BJ	Binder jetting
CF	Carbon fiber
CO	Carbon monoxide
CO_2	Carbon dioxide
D	Workpiece diameter
DED	Directed energy deposition
FDM	Fused deposition modeling
FFF	Fused filament fabrication
h	Strand height
k_{mat}	Material constant
$\dot{m}_i$	Mass flow inside the extruder
$\dot{m}_o$	Mass flow outside the extruder
ME	Material extrusion

MFI	Mel flow index
MJ	Material jetting
n_i:	Extruder speed
ρ	Density
PBF	Powder bed fusion
PLA	Polylactic acid
PK	Aliphatic polyketone
SL	Sheet lamination
T_1	Extruder zone 1 temperature
T_2	Extruder zone 2 temperature
T_3	Extruder zone 3 temperature
T_4	Extruder zone 4 temperature
T_5	Extruder zone 5 temperature
T_d	Degradation temperature
T_m	Melting temperature
v_r	Table speed
$\dot{V}_i$	Volume flow inside the extruder
$\dot{V}_o$	Volume flow outside the extruder

Chapter I: Introduction

1.1 Motivation of Work

The petrochemical industry is a key global sector, producing a wide range of petrochemical products such as plastics, pharmaceuticals, fertilizers and different textile items. (Alsabri et al., 2021). This industry has experienced sustained growth over the past 20 years. Figure 1.1 illustrates the increase in production capacity and the number of polymer products in the Middle East from 2005 to 2016 (Gulf Petrochemicals &Chemicals Association, 2016). However, the rise in plastic production is a major factor contributing to greenhouse gas emissions. This is because over 99% of plastics are derived from fossil fuel feedstocks, making plastic production one of the fastest-growing forms of petroleum consumption globally (Feit S, 2019).

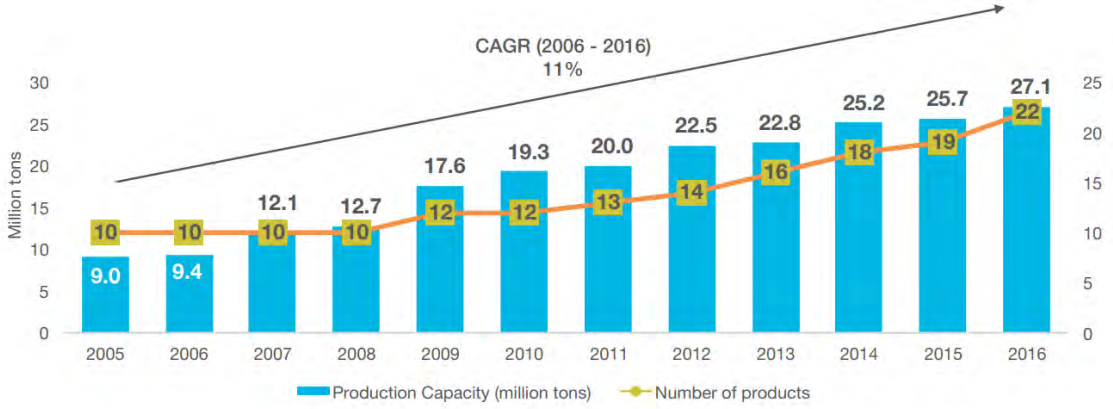

Figure 1.1. Polymers production capacity and number of products in the middle east from 2005 to 2016 (Gulf Petrochemicals &Chemicals Association, 2016).

In the 2015 Paris Climate Agreement, nations committed to keeping global warming significantly below 2 degrees Celsius and striving to limit temperature rise to less than 1.5 °C. In 2018, the Intergovernmental Panel on Climate Change concluded that to keep warming below the 1.5 °C threshold, global greenhouse gas emissions must be reduced by 45% by 2030, with the goal of reaching emissions net zero by 2050 at the latest. Figure 1.2 shows a projection of CO emissions for the year 2050 (Feit S, 2019).

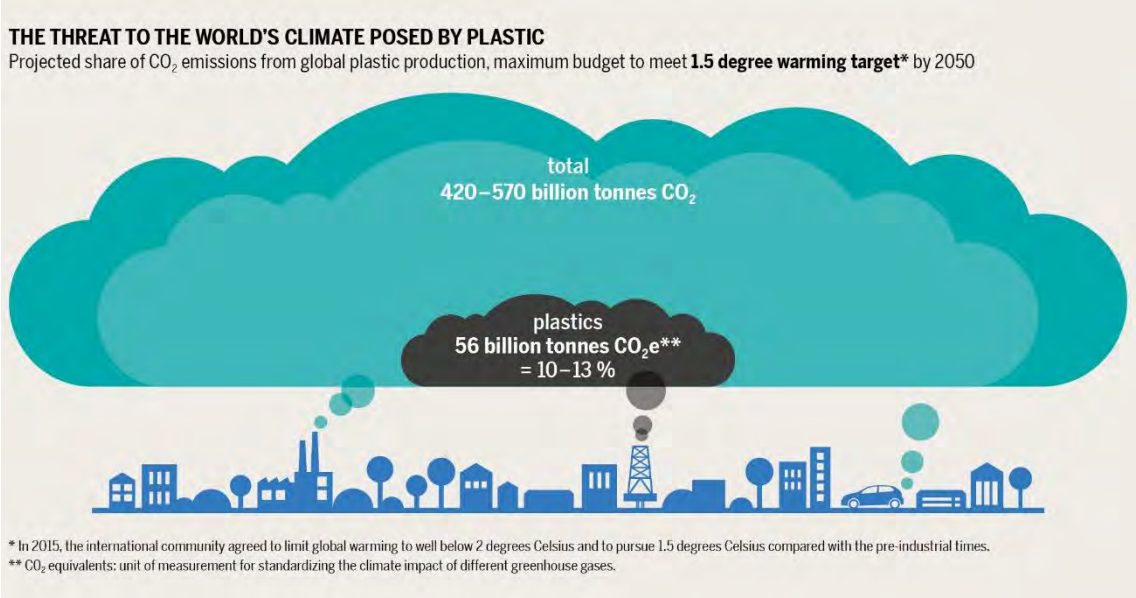

Figure 1.2. Projected CO_2 emissions from global plastic production by 2050 (Feit S, 2019).

At every stage of the plastic life cycle, from the extraction and refining of fossil fuels to the production, disposal and incineration of plastic resins, carbon dioxide, methane and other greenhouse gases are released. This greatly affects efforts to achieve global climate goals. To avoid exceeding the 1.5 °C temperature rise limit, total emissions must remain within the shrinking budget of 420-570 billion tons of carbon dioxide (Feit S, 2019).

For this reason, there is an increasing demand for environmentally friendly polymers to help mitigate environmental pollution (Labus Zlatanovic et al., 2023). Aliphatic Polyketone (PK) is a new environmentally friendly polymer made from carbon monoxide (CO), with applications in various areas including packaging, fibers, and technical products. Thanks to its excellent combination of mechanical properties and high chemical resistance, PK shows significant promise as a high-performance and versatile polymeric material. However, challenges arise in its production attributable to its limited thermal stability (Labus Zlatanovic et al., 2023).

1.2 General objective

The main objective is to assess the feasibility of producing stable parts from two different types of aliphatic polyketones utilizing screw extrusion-based additive manufacturing. Additionally, this study aims to identify the optimal operating parameters for the additive production of aliphatic polyketones and to compare the results obtained for each type of material.

1.3 Specific objectives

To achieve this general objective, the following specific objectives are proposed:

- Realize a comprehensive literature review including the extrusion-based additive manufacturing process, polyketone characteristics, and their behavior during processing.
- Optimize operating parameters for a screw extrusion-based additive manufacturing process for 2 types of aliphatic polyketone on a newly developed extruder.
- Perform thermal, microstructural, and mechanical characterization of the obtained samples.
- Establish correlations between parameters, materials, process temperatures, and properties through rigorous analysis of the results.

Chapter II: Literature review

2.1 Polyketone (PK)

Polyketones are a class of high-performance polymers characterized by alternating carbonyl and hydrocarbon groups (Melton et al., n.d.). They are subdivided into aliphatic and aromatic polyketones according to the nature of the hydrocarbon groups in their main structure. Both types have garnered significant interest due to their distinct properties and potential uses across various industries. (Al-Muaikel, 2011; Marklund et al., n.d.; Matsumoto et al., 2020).

2.1.1 Aromatic Polyketone

Aromatic polyketones are a class of aromatic polymers characterized by ketonic carbonyl groups as the primary linkage within the main aromatic polymer chain. While numerous examples of aromatic poly (ether ketones) have been documented, nearly all belong to the "aromatic poly (ether ketones)" category (Yonezawa & Okamoto, 2009).

PEEK, a poly (ether ether ketone), is a prominent example of aromatic polymers in this category, known as a super engineering plastic because of its outstanding thermal stability, mechanical strength, and chemical resistance. (Yonezawa & Okamoto, 2009). Figure 2.1 illustrates the structure of PEEK, indicating that its properties may be more closely associated with the aromatic ether component rather than the aromatic ketone.

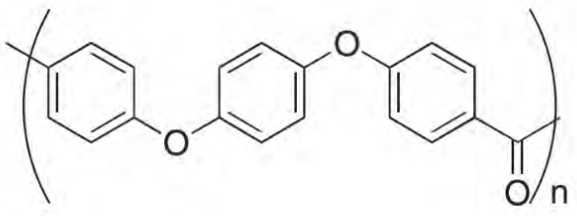

Figure 2.1. Structure of PEEK (Yonezawa & Okamoto, 2009).

Furthermore, aromatic polymers that consist solely of aromatic rings and ketonic carbonyl groups as the predominant linkages in the main chain are classified as wholly aromatic polyketones. (Gu et al., 2021). Figure 2.2 illustrates the structure of wholly aromatic polyketone. In wholly aromatic polyketones, the absence of ether bonds in the

main chain leads to a more rigid structure and enhanced thermal stability. (Gu et al., 2021).

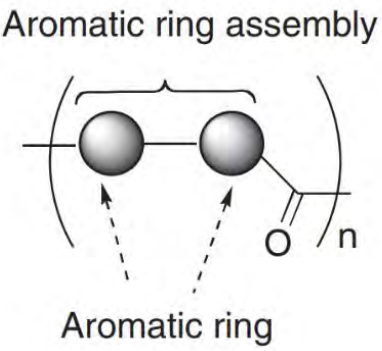

Figure 2.2. Structure of wholly aromatic polyketone (Yonezawa & Okamoto, 2009)

2.1.2 Aliphatic Polyketone

Aliphatic polyketone (PK) is a relatively new type of semicrystalline polymer known for their enhanced chemical, thermal, and mechanical properties (Lin et al., 2020). This semicrystalline polymer belongs to the group of high-performance thermoplastic polymers and are obtained through the polymerization of α-olefins and carbon monoxide (CO) to create a copolymer of ethylene-CO (ECO) or terpolymerization of ethylene-propylene-CO (EPCO) as shown in figure 2.3 (Bae et al., 2014). Due to the use of carbon monoxide (CO) as a raw material, this polymer can be considered environmentally friendly. This is because carbon monoxide (CO) waste is used, which is actually a toxic gas and air pollutant (Jung et al., 2018).

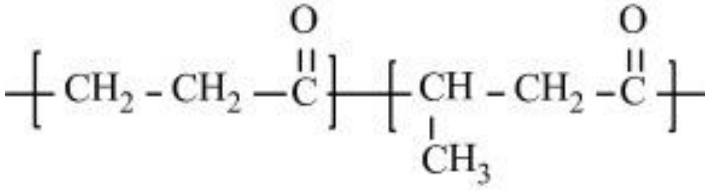

Figure 2.3. Structure of ethylene-propylene-CO aliphatic polyketone (Wang et al., 2016).

In addition, the inclusion of polar carbonyl groups within the main chain promotes important intra- and intermolecular interactions, thus improving the physical and chemical properties of the polymer. These intermolecular polar forces contribute to a

semicrystalline polymer characterized by a glass transition temperature of 15°C. (Zuiderduin et al., 2005). Therefore, these polymers typically exhibit excellent chemical and thermal resistance, along with strong mechanical properties and effective gas barrier properties (Wang et al., 2016). According to Zuiderduin et al. (2003), PK demonstrates impact resistance and chemical resistance that are 2.3 and 2.5 times superior to nylon, a common engineering plastic. These exceptional properties position PK with substantial commercial promise across various applications such as engineering, barrier packaging, fibers, and blends (Lagaron et al., n.d.).

Despite these amazing physical properties and environmental friendliness, aliphatic polyketone presents some challenges such as low elastic modulus and thermal instability at elevated temperatures (> 220°C) (Cho et al., 2019). This is due to the polymer's relatively high melting temperature (~260°C), which is approximately 125°C higher than the melting temperature of polyethylene (Zuiderduin et al., 2003). The high crystallinity of polyketones makes them difficult to process without degradation. At higher temperatures, such as during melt processing, polyketones can undergo aldol condensation reactions both between molecules and within the same molecule. Interactions between molecules can cause degradation (cross-linking), causing an increase in melt viscosity that restricts the processing range of these polymers. These reactions are usually catalyzed by impurities such as salts (ions) and residual catalysts. (Zuiderduin et al., 2003).

For this reason, several efforts were made to overcome these problems by manufacturing PK-based composites (Stadlbauer et al., n.d.). Adding other substances such as polymers, reinforcing fibers or micro- and/or nanofillers to the PK matrix is an effective strategy to develop new PK-derived materials, aimed at achieving specific characteristics and substantial improvements in properties (Yang et al., 2018).

2.1.3 PK-based composites

PK-based composites refer to the use of filler materials to improve the mechanical, thermal and electrical properties of polyketone. Zuiderduin et al. (2006) reported the impact of precipitated calcium carbonate (CaCO3) particles on the toughness characteristics of aliphatic polyketones. It was found that while the thermal properties of the matrix remained constant, the addition of CaCO3 resulted in an increase in modulus

and a decrease in yield strength. This decrease in the yield strength can be attributed to the separation of the particles from the matrix. The figure 2.4 illustrates the toughening mechanism with rigid particles, in which the CaCO3 content has been compounded and injection molded.

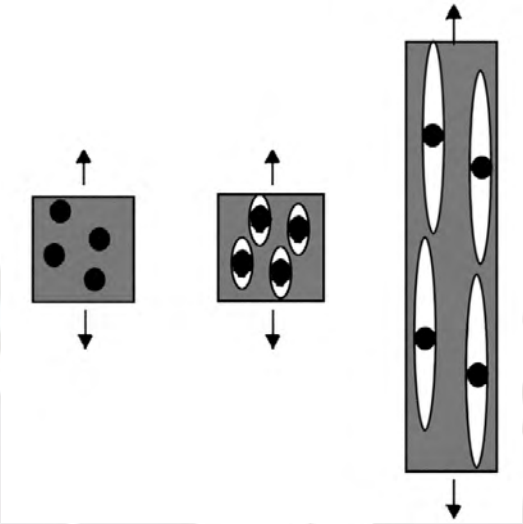

Figure 2.4. Toughening mechanism with rigid particles
(Zuiderduin et al., 2006).

On the other hand, Lim et al. (2015) reported the creation of composites based on PK using a polymer powder coating method, incorporating carbon nanomaterials like carbon nanotubes (CNTs), graphene oxide (GO), and antioxidant-modified GOs as fillers. PK composites incorporating carbon nanomaterials exhibited significantly improved thermal stability and mechanical properties compared to pure PK. Specifically, antioxidant-modified graphene oxide (GO) was shown to be more effective in improving the thermal properties of PK than carbon nanotubes (CNTs) and unmodified GO. The superior thermal stability and mechanical properties of antioxidant-modified GO can be attributed to the synergistic effects of antioxidant functional groups and rigid conjugated carbon structures present in GO, which possesses an ultrathin sheet morphology. (Lim et al., 2015). The figure 2.5 provides a schematic representation of the antioxidant mechanism in PK composites incorporating antioxidant-modified graphene oxides (GOs).

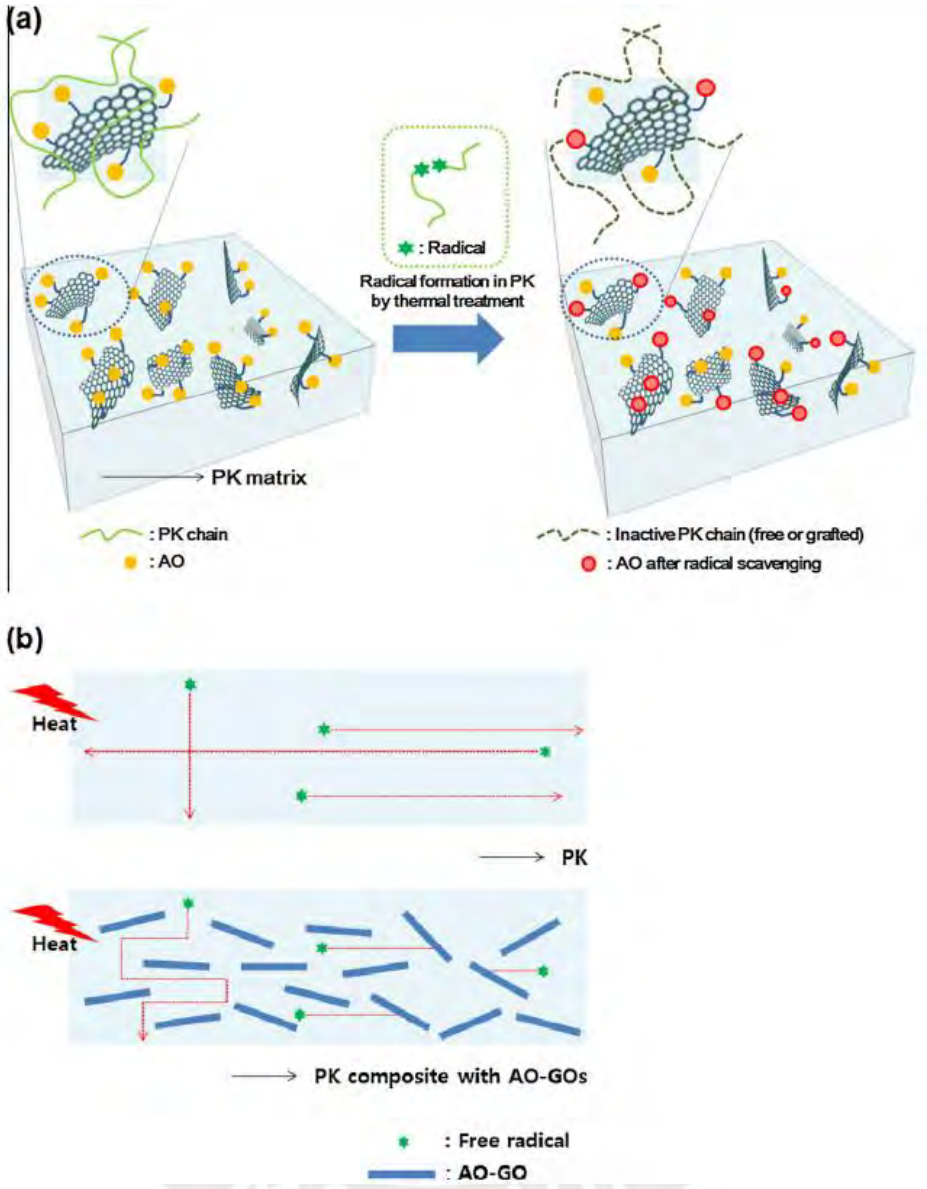

Figure 2.5. Schematic diagram of the antioxidant mechanism of AO-GOs: (a) creation of inactive polymer chains by radical scavenging of GO and the antioxidant and (b) barrier effect of AO-GOs within PK matrix (Lim et al., 2015).

Finally, Cho et al. (2019) investigated the impact of carbon fiber (CF) content on the mechanical properties of PK-based composites. It was found that integrating carbon fibers into PK enhances the thermal stability, electrical conductivity, and mechanical characteristics of the composites. Figure 2.6 illustrates the production process of carbon fiber (CF)-reinforced polyketone (PK) composites.

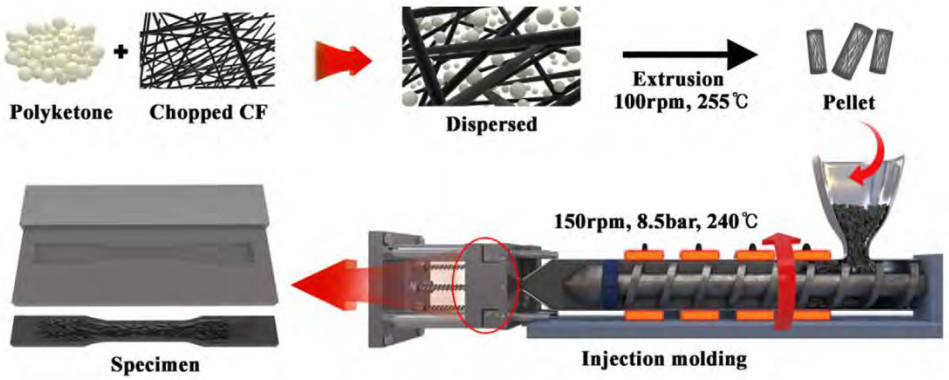

Figure 2.6. Manufacturing process of carbon fiber (CF) - reinforced polyketone (PK) composites (Cho et al., 2019).

In recent years, fiber-reinforced polymer composites (FRPC) have gained much attention due to their simple manufacturing process and excellent properties (Tang & Jeong, 2023). Currently, more studies are being carried out focused on improving the properties of aliphatic polyketones, since it is a material with a great economic and environmental potential.

2.1.4 Applications of PK-based materials

As discussed in the previous section, PK-based materials have several advantageous characteristics such as good mechanical and chemical properties, low permeability and environmentally friendly behavior. The advent of new technologies is expected to lead to growth in the market for PK materials, including PK-based composites, in different sectors such as packaging, fibers, automotive, electronics, biomedical, etc. (Mi HL, 2016).

These materials have favorable mechanical properties along with lightweight characteristics, making them well suited for a wide variety of structural applications in the construction sector. These applications include industrial fuel systems, filters, pipes and pipe fittings to pumps, chemical transfer liners and containment systems (Gergen WP and Machado JM., 1990; Gergen WP, 1991).

Besides, its robust toughness and strength are used in internal and external automotive components, such as sucker rods, mirror frames and valve cover, as well as in mechanical molds (George ER, 1989, 1992).

Additionally, their exceptional wear resistance expands their suitability for transmission applications and automotive components, such as fluid handling systems, gears, bearings, hoses, and washers (Mi HL, 2016).

Finally, its flame-retardant properties allow for its potential use in electrical connectors, enclosures, and related applications. With demonstrated biological safety, including the absence of cytotoxicity, genotoxicity, allergenicity, irritation, and systemic toxicity, these materials show promise as replacements for non-degradable polymeric biomaterials. Also, they can serve as coatings for wires and cables, whether on glass or metal substrates (Mi HL, 2016). In summary, the main applications of PK are listed in table 2.1.

Table 2.1. Main applications of PK-based materials (Yang et al., 2018).

Sectors	**Applications**
Packaging	• Storage containers for liquid hydrocarbons. • Packaging designed for hot filling or sterilization in food or medical fields.
Fibers	• Fibrous materials utilized for creating ropes, fishing lines, and brushes. • Strengthening mechanical rubber goods such as tire cords through reinforcement. • Porous membranes employed as supportive structures in the production of forward osmosis membranes.
Industrial	• Components for industrial fuel systems, encompassing filters, pipes, pipe fittings, pumps, and related equipment. • Industrial uses including handcart wheel structures, brakes, gears, washers, bearings, and more.
Automotive	• Automotive applications in both interior and exterior components like sucker rods and mirror frames.
Electrics and Electronics	• Housing for connectors and switches.
Biomaterials	• Medical applications in ophthalmology, dentistry, bone repair, and drug delivery systems.
Coating	• Coatings for wires and cables used with glass and metal.

2.2 Additive Manufacturing (AM)

Additive manufacturing (AM) is defined according to the International Standards Organization/American Society for Materials Testing and Standards (ISO/ASTM 52900:2015) as a process of joining materials to achieve 3D parts with desired geometries, usually strand by strand (ASTM. ISO/ASTM 52900:2015, 2015).

In addition, ISO/ASTM 52900:2015 identifies all additive manufacturing processes into seven main categories (Daminabo et al., 2020). These main categories are the following (Ligon et al., 2017):

- Material extrusion (ME): This AM technique heats material and precisely deposits it through a nozzle to create layers for a 3D component.
- Material jetting (MJ): This AM technique involves depositing droplets of build material, such as photopolymers or thermoplastics, to construct thin layers of a 3D object.
- Binder jetting (BJ): This AM technique uses a liquid bonding agent to fuse powder materials together.
- Sheet lamination (SL): This AM technique bonds together sheets or foils of material to form a solid object.
- Vat Photopolymerization (VP): This AM technique cures liquid photopolymer resin in a vat using light to trigger polymerization.
- Powder bed fusion (PBF): This AM technique selectively fuses specific areas of a powder bed using thermal energy, typically from a laser or electron beam.
- Directed energy deposition (DED): This AM technique employs concentrated thermal energy, such as from a laser or plasma arc, to melt materials as they are deposited. Currently, this process is primarily used for metals.

In summary, all additive manufacturing processes can be classified into three main groups: solid, liquid and powder, depending on the physical form of the raw materials used (C.K. Chua, 2014). Figure 2.7 presents the classification and different types of additive manufacturing processes, along with a comparison focusing on build volume, material options, and respective advantages and limitations.(Altıparmak & Xiao, 2021).

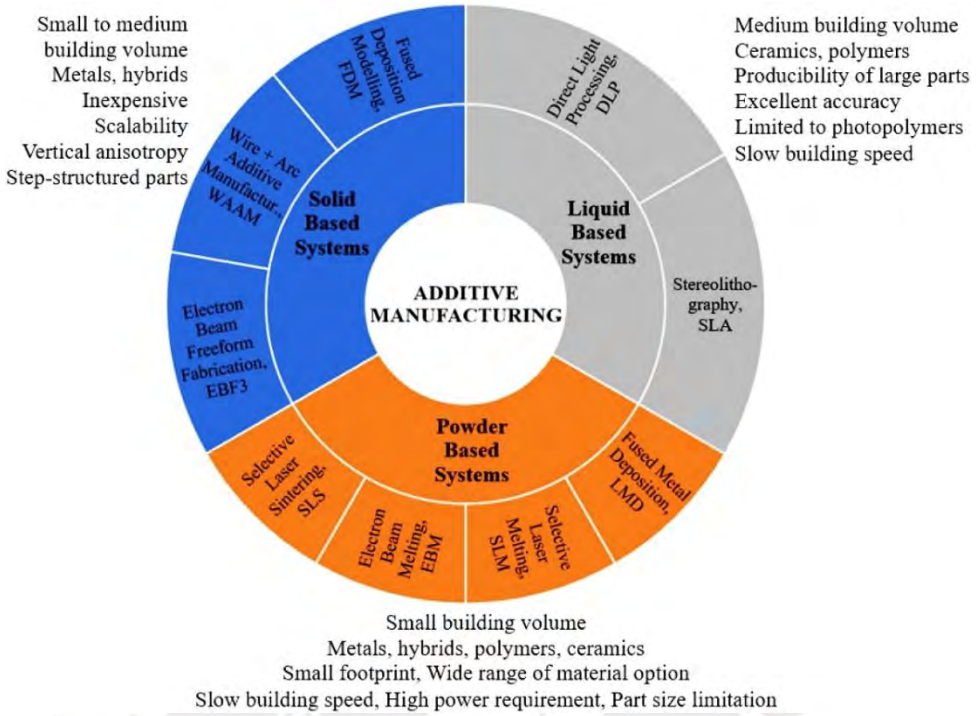

Figure 2.7. Classification and comparison of AM processes (Altıparmak & Xiao, 2021).

2.2.1 Advantages and limitations of AM processes

Additive Manufacturing (AM) has gained value in market growth in recent decades due to a wide range of potential advantages over conventional manufacturing processes. Additive manufacturing processes make it easier to manufacture complex designs such as deep channels, complex shapes, components with improved strength-to-weight ratios, blind holes, and parts that would otherwise require multiple assembly or joining steps (Joshi & Sheikh, 2015).

One of the potential benefits is that additive manufacturing processes can reduce raw material waste by almost 40% compared to conventional manufacturing methods, with 95% to 98% of the waste material being recyclable (Petrovic et al., 2011). This is largely because the additive manufacturing method is an automated and simplified system that just requires CAD software to produce physical objects, contrasting to the extensive labor required for conventional manufacturing (Berman et al., 2012). Thanks to these capabilities, additive manufacturing can be seen as a tool that improves design flexibility, allowing manufacturers to create integrated parts in innovative ways, even at low volumes and at reduced cost (Bikas et al., 2016).

Another benefit of this technology is its environmental friendliness, as additive manufacturing can produce lightweight components with strong structural integrity, contributing to green practices (Li et al., 2019). This technology integrates easily with both traditional subtractive manufacturing and other additive manufacturing processes, enabling the development of hybrid additive manufacturing solutions that improve the properties of final products produced solely through conventional subtractive manufacturing or additive manufacturing processes (Altıparmak et al., 2021).

Nevertheless, Additive Manufacturing (AM) has some limitations such as lack of globally accepted certification and standardization, elevated material cost, limited component size, and relatively slow production speed (Ford & Despeisse, 2016; Uriondo et al., 2015). The main advantages and limitations of AM processes are shown in Table 2.2.

Table 2.2. Advantages and limitations of AM processes (Altıparmak & Xiao, 2021).

Advantages	Limitations
• Minimization of production costs.	• High initial investment costs for AM equipment, materials, and software.
• Creation of unique and complex shapes (design flexibility).	• Limited reliability in terms of mass production.
• Reduction in the need for part assembly.	• Absence of widespread certifications and standardization.
• Minimization of material waste.	• Constraints on component size and build volume.
• Capability for environmentally friendly manufacturing.	• Lower production speed compared to subtractive manufacturing.
• Possibility of producing lightweight components.	• Expensive for large-scale production.
• Elimination of tooling and fixturing requirements.	• Metallurgical imperfections like porosity or hot cracking.

In the following section, material extrusion (ME) will be analyzed in detail.

2.3 Extrusion-based additive manufacturing

In contrast to liquid- and powder-based additive manufacturing processes, extrusion-based additive manufacturing is simple to set up, making it feasible in-home environments with minimal equipment and energy costs. Consequently, this technology has been adopted by a wide range of users, from hobbyists to large-scale manufacturers in various industrial sectors (Mohd Pu'ad et al., 2019).

In extrusion-based additive manufacturing processes, unlike liquid- and powder-based methods, a feed material is heated to form a viscoelastic melt (Joseph Rey et al., 2021). This molten material flows with a high viscosity as it's pushed through the extruder's nozzle (Gibson et al., 2021). Typically, the material being extruded is considered a Newtonian fluid, meaning that its viscosity remains constant regardless of the shear strain rate, and there is a linear correlation between shear rate and stress (Herderick et al., 2016). Currently, most extrusion-based additive manufacturing processes use a single print head. However, there is a growing prevalence of machines equipped with multiple print heads, which facilitate the manufacturing of multi-material components (Sames et al., 2016).

Besides, extrusion-based additive manufacturing processes employ two main methods to facilitate the adhesion of successive printed strands. The predominant approach involves controlling the temperature of the extruded material: it is liquefied and extruded in a softened or molten state so that it flows through the nozzle and deposits on the build table or pre-printed strand before solidifying. (Altıparmak et al., 2022). The second approach uses chemical alterations to aid in the solidification and subsequent joining of sequentially deposited strands. For example, in processes such as direct ink writing (DIW), extruded additive manufacturing material (typically ink or paste) is deposited on previously placed strands, initiating chemical bonding and cross-linking between strands immediately. (Baiano, 2022; Gonzalez-Gutierrez et al., 2018).

On the other hand, all extrusion-based additive manufacturing processes include features that differentiate them from liquid- and powder-based methods, as follows: (Altıparmak et al., 2022):

- Material loading: A continuous feed (such as filament, wire, or paste) maintains a constant inlet pressure at the nozzle, allowing molten material to be extruded

and deposited onto previously printed strands on a build table. This contrasts with liquid- and powder-based processes, where parts are typically built within a resin tank or powder bed that is gradually lowered to allow the addition of new material on top of the previously deposited strand.

- Material liquefaction: The molten material is held within the print head, where it is continuously heated by a heat source, usually heating coils surrounding the reservoir.
- Extrusion of the liquefied material: Nozzle size has a notable impact on the quality of printed parts. A larger nozzle increases the rate at which material is deposited and reduces the time required for manufacturing, but it also decreases the dimensional accuracy of the printed product.
- Solidification and bonding of the strands to form a solid dense structure: Ideally, the shape and dimensions of the printed part should closely match those of its CAD model. However, during cooling and drying, surface tension and gravity may slightly alter the dimensions of extruded materials. Depending on the coefficient of thermal expansion, the material may shrink and develop porosity as it solidifies. To mitigate this, the cooling rate can be slowed down or the temperature difference between the print head and the freshly printed strands can be reduced.

2.3.1 Classification of extrusion-based AM processes

Extrusion-based additive manufacturing processes are categorized based on the mechanism used for extrusion, which may involve filament, plunger or syringe, or screw. (Nurhudan et al., 2021). These types of mechanisms are detailed below.

2.3.1.1 Filament-based extrusion

Stratasys, Ltd. was the first to patent extrusion technology with filament-based materials. Fused Filament Fabrication (FFF) is another type of Fused Deposition Modeling (FDM), whose material type is filament. FDM was the pioneering extrusion-based additive manufacturing process and remains the most widely used, followed by FFF. (Altıparmak et al., 2022). The main distinction between FDM and FFF occurs in the operating environment. FDM operates within a closed, thermally insulated chamber that maintains a constant temperature. This configuration improves the mechanical properties of printed materials and improves inter-strand adhesion but imposes limitations on the maximum

dimensions of printable parts. In contrast, FFF technology operates in an open environment where materials are exposed to fluctuating temperatures, which can lead to residual stresses and weaker strand adhesion (Gonzalez-Gutierrez et al., 2018). To mitigate this, the build table is heated before printing begins to minimize the temperature difference between it and the initial molten strand. This preheating ensures better adhesion between the first printed strand and the table, which is essential to maintain structural integrity and dimensional accuracy. As a result, FFF has become the most adopted single-material extrusion process, attractive to both hobbyists and industries due to the variety of filament materials available, the cost-effectiveness of the process, and the lack of size restrictions of construction (Spoerk et al., 2018).

In this filament-based process, the material is driven through a roller extruder mechanism to guide the filament towards the nozzle (Agarwala et al., 1996). The main components of extrusion using filament-based methods are illustrated in Figure 2.8.

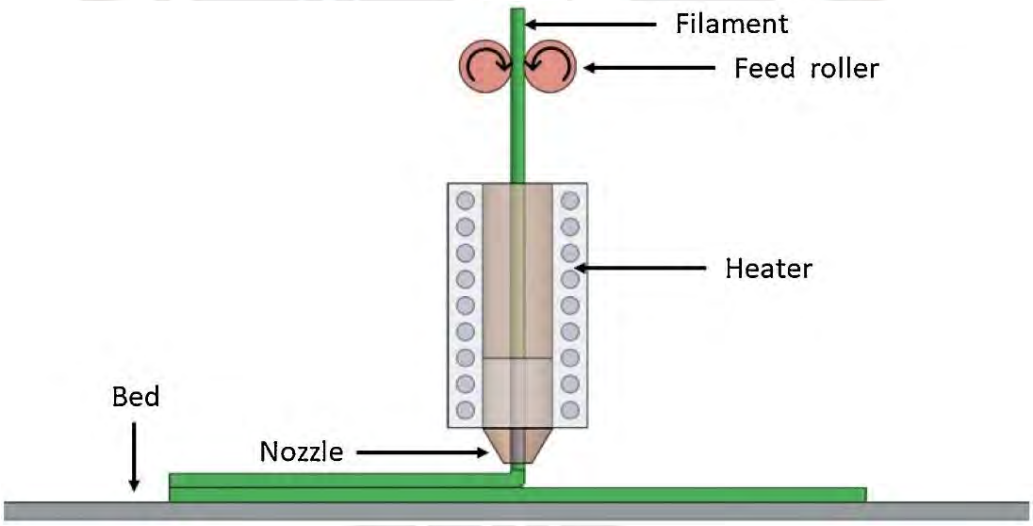

Figure 2.8. Filament-based extrusion mechanism (Nurhudan et al., 2021).

The feed roller pushes the material into the heater, which melts the material and directs it to the nozzle. The nozzle then discharges the material strand-by-strand onto the table. The flow printing process starts with the feed roller pushing the filament into the heating chamber. The temperature must exceed the material's melting point to ensure it flows into the nozzle. As this occurs, the material follows a predefined path to create the object (Nurhudan et al., 2021). These requirements are primarily met by a limited range of materials, predominantly thermoplastics (Gonzalez-Gutierrez et al., 2018). PLA and ABS

are the most used filament materials in FFF, although other commercially available thermoplastics can also be used with this technology (Gao et al., 2015; Kamaal et al., 2021; Mousapour et al., 2021).

2.3.1.2 Syringe or Plunger-based extrusion

In this form of extrusion-based additive manufacturing, rather than using feed rollers as in filament-based processes, an actuator-driven plunger or syringe is used to control the flow of material (Nurhudan et al., 2021). The main components of extrusion using syringe or plunger-based methods are illustrated in Figure 2.9.

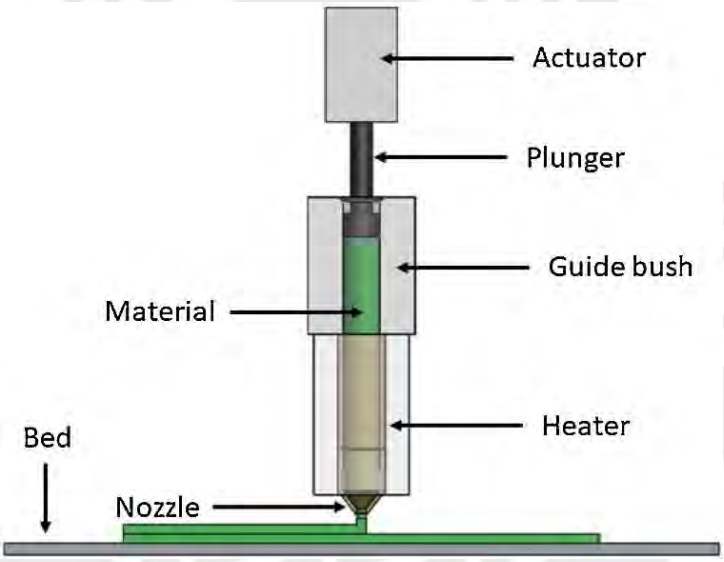

Figure 2.9. Syringe or plunger-based extrusion mechanism (Nurhudan et al., 2021).

This mechanism is used with print-compatible raw materials, such as inherently fluid-like materials (e.g., pastes) and additive manufacturing materials with low melting points. A plunger or syringe is used to push the feed material into the heating chamber of the print head, where it is subsequently extruded through the nozzle for deposit onto the build table or previously printed strands (Gonzalez-Gutierrez et al., 2018). The printing process starts immediately after the material passes through the guide bushing (Nurhudan et al., 2021). Furthermore, it is not necessary for the material to melt completely, since high pressures facilitate extrusion at temperatures below its melting point. This mechanism allows the deposition of additive manufacturing materials at lower

process temperatures, particularly when the raw material, such as PLA, has a relatively low melting point (Altıparmak et al., 2022).

2.3.1.3 Screw-based extrusion

Strict filament material requirements have led manufacturers to adopt an alternative mechanism known as screw-based extrusion additive manufacturing. This approach allows the use of granules, typically spherical in shape, instead of filaments (Gonzalez-Gutierrez et al., 2018). The main components of extrusion using screw-based mechanism are illustrated in Figure 2.10.

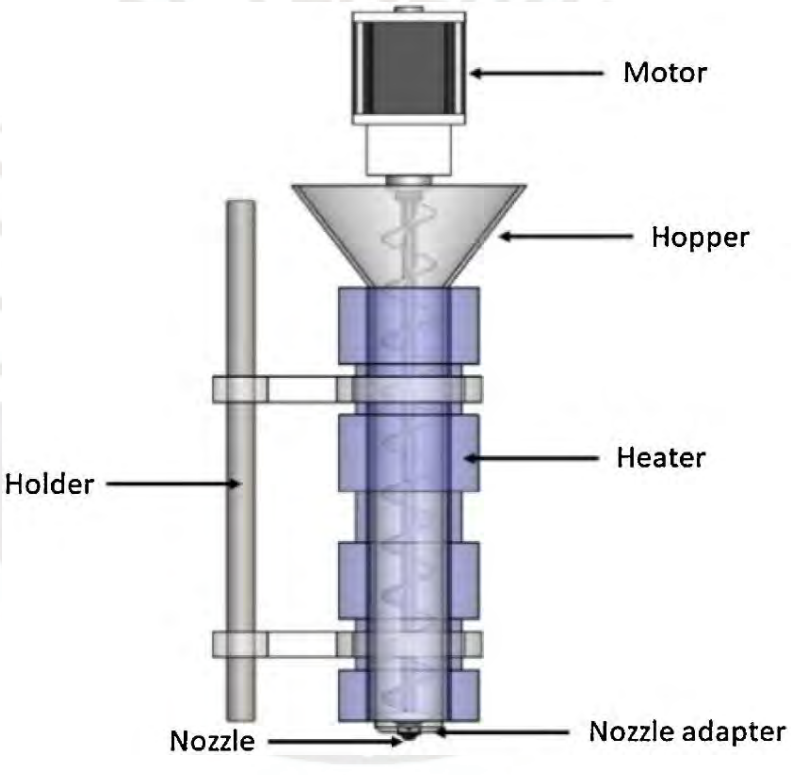

Figure 2.10. Screw-based extrusion mechanism (Nurhudan et al., 2021).

The granular feedstock enters the extruder system through the hopper (Nurhudan et al., 2021). Inside the extruder barrel, the granules are transported to a melting zone where they soften but do not completely melt, as a result of friction and applied heat. As the material progresses along the barrel, it undergoes increasing pressure and temperature. The rotating screw within the barrel serves to advance the material while simultaneously compressing it against the barrel walls (He et al., 2021; Tseng et al., 2018). The molten

material passes through a nozzle at the end of the barrel. Once the material exits the nozzle, it is extruded as a continuous stream of molten material.

This process is regarded as the most stable due to its consistently secure operation. Additionally, the temperature must exceed the material's melting point to ensure its flow through the nozzle. Once this occurs, the material follows a predetermined path to create the object as planned (Nurhudan et al., 2021).

2.3.2 Key process parameters for screw-based extrusion

2.3.2.1 Printing temperature

Temperature settings have an important effect in the screw-based extrusion process in additive manufacturing. The precise control of temperature across different zones of the extruder affects the quality, consistency, and mechanical characteristics of the final printed product (Ambade et al., 2023). One of the most important aspects to consider is thermal degradation, that is, the properties of the material deteriorate due to the effect of high temperatures. Different materials have specific thermal degradation points.

In addition, the extrusion temperature plays a critical role in strand adhesion, which directly impacts the structural integrity and mechanical properties of the part. The thermal energy of the material being extruded promotes bonding between the strands. When the temperature exceeds the glass transition temperature of the material, the adhesive bond between the strands improves. Maintaining a high extrusion temperature (while ensuring it does not exceed the material degradation temperature) promotes strong bonds. The strength of these joints directly correlates with the mechanical durability of the part (Yadav et al., 2022).

2.3.2.2 Printing speed

Screw and table speeds are 2 important parameters connected with printing speed in additive manufacturing. These parameters directly affect the reliability of the printed parts (Ambade et al., 2023). There are some investigations regarding the influence of printing speed in additive manufacturing. For instance, Yao et al. (2020), found that in FDM printing of PLA components, higher printing speeds generally lead to lower tensile and

compressive strengths. The study highlighted that the highest tensile and compressive strengths were observed in samples with a strand height of 0.15 mm, an infill density of 100% and a printing speed of 30 mm/s. Furthermore, the research indicated that the impact of strand height and filler density on tensile and compressive strength is significantly greater than that of printing speed.

Although lower printing speeds usually have a better effect on the quality of the printed parts, these speeds should not be too low as they generate other problems during printing such as warping specially in the first strands due to the rapid cooling of the part. Warping in additive manufacturing refers to the unwanted bending or distortion of a printed part, particularly in the base strands, which can cause the part to lift off the table or develop a curved, uneven surface (Brion et al., 2022).

2.3.2.3 Nozzle diameter

Nozzle diameter is also an important parameter in 3D printing. The nozzle diameter determines the volume of material that can be extruded. A larger nozzle diameter allows for a higher flow rate, increasing the production speed (Czyżewski et al., 2022). Besides, smaller nozzle diameters require higher extrusion pressures to maintain the same flow rate, which can affect the performance and wear of the extruder (Xu et al., 2022). However, larger nozzle diameter also increases the amount of molten material and therefore the temperature between strands, which could generate geometric deviation problems such as the sinking of the piece due to excess heat.

In recent years, extensive research has focused on enhancing the performance of the extrusion nozzle. For instance, Jeon et al. (2020) investigated how nozzle temperature affects the emission rate of materials. It was found that at an operating temperature of 185 °C, the emission rate ranged from 107 to 109 particles/min, while at 290 °C, the emission rate increased to 1011 particles/min. On the other hand, S. Ding et al. (2019) examined how nozzle temperature influences the mechanical properties of 3D printed parts. The flexural strength of polyetherimide (PEI) printed parts was found to increase with higher nozzle temperatures, between 360 and 420 °C.

2.3.3 Swell effect

The swell effect, also known as die swell or extrudate swell, is a phenomenon in extrusion-based additive manufacturing (AM) where the extruded material expands upon exiting the nozzle. This expansion occurs due to the relaxation of internal stresses accumulated in the material as it is forced through the nozzle (Colon et al., 2023).

Inside the extruder, the material is heated and pressurized. As it is pushed through the nozzle, the material flows and undergoes deformation due to shear forces. Upon exiting the nozzle, the material experiences a sudden release of pressure. This causes the internal stresses to relax, leading to an expansion of the material. Besides, the degree of expansion depends on the characteristics of the material and the parameters used in the extrusion process. The material's elasticity causes it to swell, increasing its diameter (Smith et al., 2024).

Other rheological phenomena observed in material extrusion, which can interact with die swelling and affect part quality, include material compressibility and contact pressures. For example, die swelling affects the alignment of short fibers, resulting in increased anisotropy in the mechanical properties of extruded parts filled with short fibers. Additionally, die swelling can cause deviations in the dimensions of the extruded roads from their intended specifications (Colon et al., 2023).

2.3.4 Wear of the nozzle

A common problem in manufacturing processes is tool wear, which can lead to poor surface finish and decreased mechanical properties of the workpiece. This problem also affects additive manufacturing methods such as material extrusion. In this process, the extrusion nozzle can suffer significant wear, especially when printing with highly abrasive materials, such as carbon fiber reinforced polymers (Bianchi et al., 2024).

Nozzle wear during the 3D printing process, caused by material flow during extrusion, can create significant challenges. These challenges include increased workpiece surface roughness, decreased nozzle precision during filament deposition, decreased tool life, and incorrect filament diameter during printing (Bianchi et al., 2024). Olsson et al. (2017) observed problems with nozzle wear when using highly abrasive materials in the FFF

process. However, the study did not analyze in depth the wear of the nozzles and its relationship with the mechanical properties of the printed parts.

On the other hand, Bianchi et al. (2024) investigated how nozzle wear affects the mechanical properties of 3D printed carbon fiber reinforced polymer parts. It was found that the mechanical properties of printed parts are significantly influenced by printing time, which correlates with the degree of nozzle wear. The study highlighted that the external surfaces of the nozzle experience increased wear due to contact abrasion between the tool and the deposited extruded material, while the internal wear of the nozzle was minimal. Furthermore, the investigation confirmed that nozzle wear causes a deterioration in the quality of the surface finish of printed parts and the appearance of gaps and macro defects within the components.

Chapter III: Experimental method

3.1 Materials

This section details 2 types of aliphatic polyketones used in the form of granules by the supplier AKRO-PLASTIC GmbH. These were PK-HM 8 black (6246) and PK-VM GF 30 black (8655).

3.1.1 PK-HM 8 black (6246)

PK-HM 8 black (6246) is an unreinforced, high viscosity polyketone. The average granule size was 3.6 ± 0.39 mm as shown in Figure 3.1.

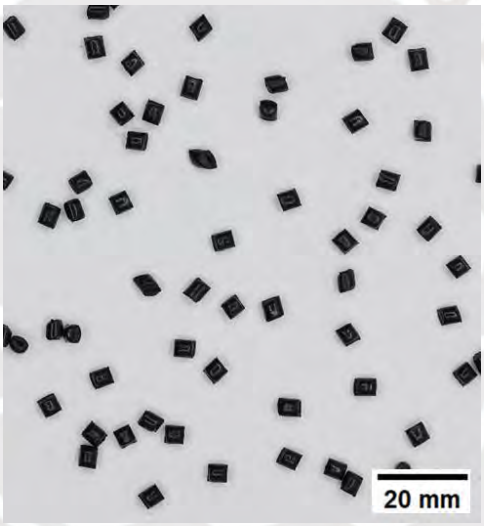

Figure 3.1. Granular material PK6246.

The main properties and recommendations given by the supplier of PK6246 are shown below (*AKROTEK PK-HM 8 Black (6246)*., n.d.):

- ✓ Tensile strength: 60 MPa
- ✓ Impact resistance: 180 kJ/m²
- ✓ Density (23 °C): 1.24 g/cm³
- ✓ Melting temperature: 220 °C
- ✓ Processing moisture: 0.02 – 0.1 %
- ✓ Melt flow index (MFI): 6 cm^3 /10 min

To determine the moisture of PK6246, SARTORIUS MA 100K instrument was used as showed in Figure 3.2. The moisture content of the PK6246 material was assessed at 105 °C for 20 minutes. The initial polyketone had a moisture level of 0.19%, and after being dried for 4 hours at 80 °C, the moisture decreased to 0.12%, which was considered acceptable by the material supplier.

Figure 3.2. SARTORIUS MA 100K instrument.

3.1.2 PK-VM GF 30 black (8655)

PK-VM GF 30 black (8655) is a 30% glass fiber reinforced polyketone with average stiffness and strength. The average granule size was 3.19 ± 0.27 mm as shown in Figure 3.3.

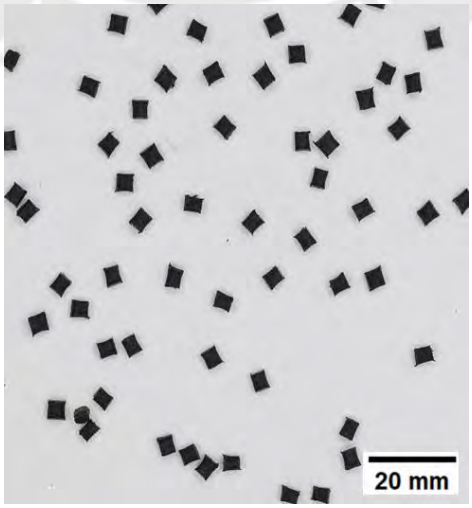

Figure 3.3. Granular material PK8655.

The main properties and recommendations given by the supplier of PK6246 are shown below (*AKROTEK PK-VM GF 30 Black (8655)*., n.d.):

- ✓ Tensile strength: 130 MPa
- ✓ Impact resistance: 70 kJ/m²
- ✓ Density (23 °C): 1,48 g/cm³
- ✓ Melting temperature: 220 °C
- ✓ Processing moisture: 0.02 – 0.1 %
- ✓ Melt flow index (MFI): 4 cm^3 /10 min

To determine the moisture of PK8655, SARTORIUS MA 100K instrument was used as well. The moisture content of the PK8655 material was assessed at 105 °C for 20 minutes. The initial polyketone had a moisture level of 0.27%, and after being dried for 4 hours at 80 °C, the moisture decreased to 0.07%, which was considered acceptable by the material supplier.

3.2 DSC and TGA analysis of PK base material

A differential scanning calorimetry instrument Netzsch DSC 204 F1 Phoenix was used to study the heat capacity and thermal transitions as shown in Figure 3.4. On the other hand, a thermogravimetric analysis instrument Netzsch TG 209 F1 Iris was used to measure the mass of the sample over time as the temperature changes as shown in Figure 3.5.

Figure 3.4. Differential Scanning Calorimetry instrument.

Figure 3.5. Thermogravimetric analysis instrument.

In addition, Figures 3.6 and 3.7 show the results of differential scanning calorimetry and thermogravimetric analysis of PK6246 granulates (base material), respectively. The melting temperature (T_m) and degradation temperature (T_d) temperatures were 256.8 °C and 340.6 °C, respectively. Likewise, other melting temperature peaks are observed due to the presence of other polymers. According to the supplier (*AKROTEK PK-HM 8 Black (6246)*., n.d.), these are Polyamide (PA) and Polyoxymethylene (POM) which were possibly used to stabilize the material.

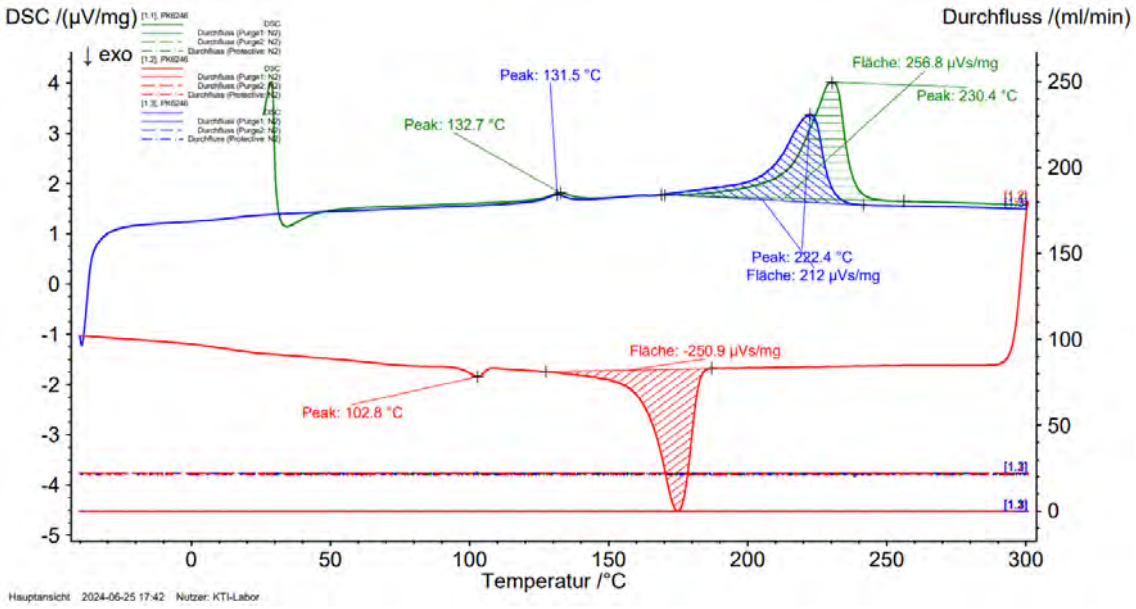

Figure 3.6. DSC thermogram of PK6246 granulates.

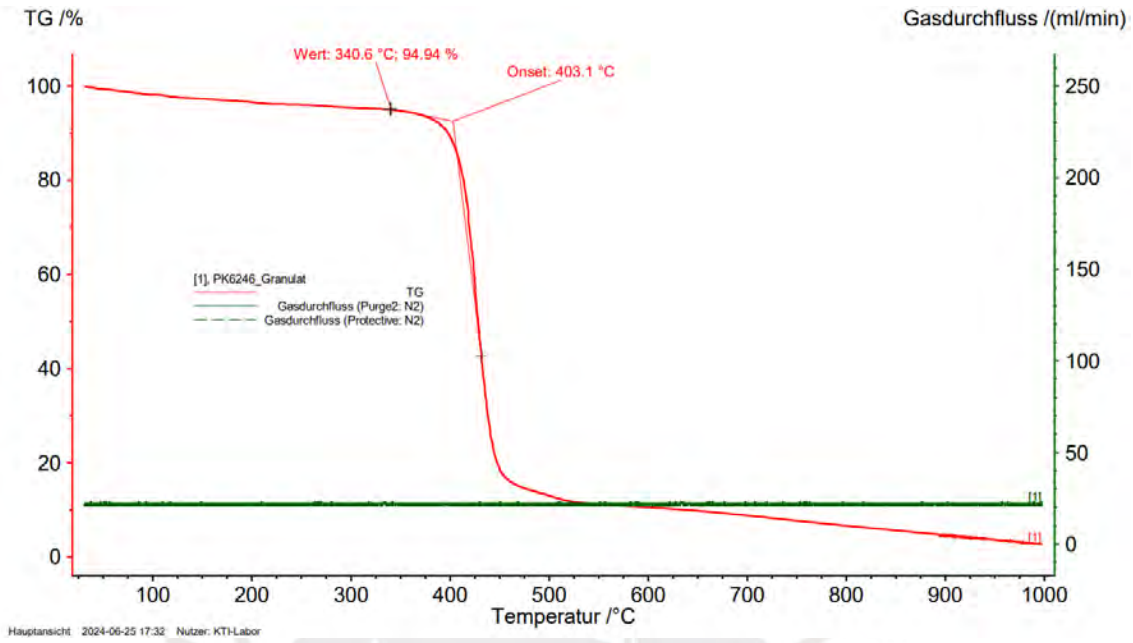

Figure 3.7. TGA thermogram of PK6246 granulates.

Furthermore, Figures 3.8 and 3.9 show the results of differential scanning calorimetry and thermogravimetric analysis of PK8655 granulates (base material), respectively. The T_m and T_d were 229.2 °C and 328.6 °C, respectively. Likewise, other melting temperature peaks are also observed due to the presence of other polymers. According to the supplier (*AKROTEK PK-VM GF 30 Black (8655)*., n.d.), these are also Polyamide (PA) and Polyoxymethylene (POM) which were possibly used to stabilize the material.

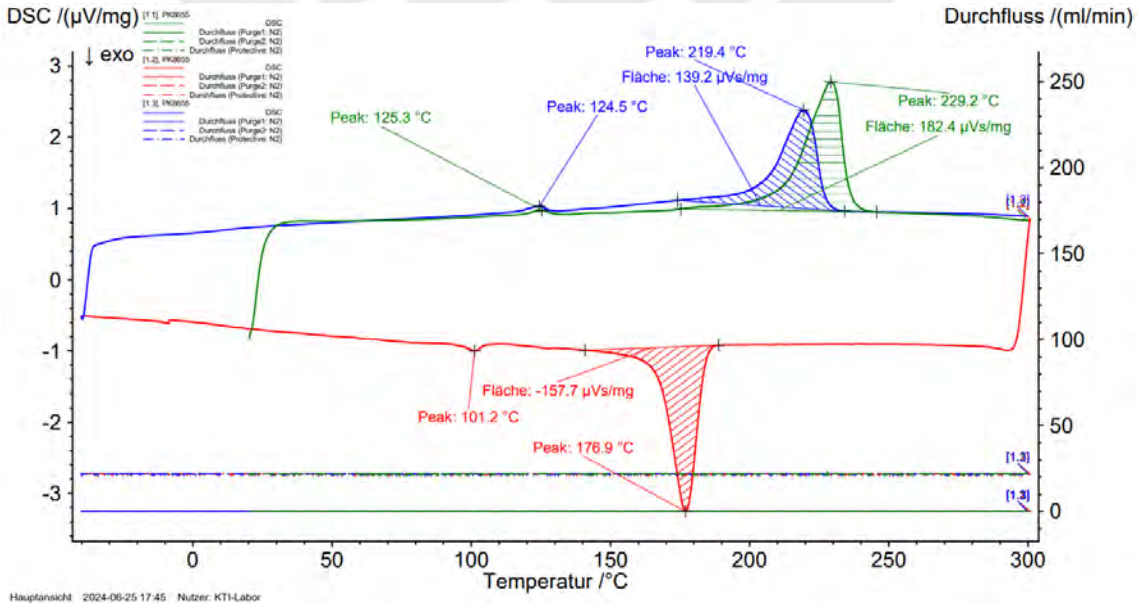

Figure 3.8. DSC thermogram of PK8655 granulates.

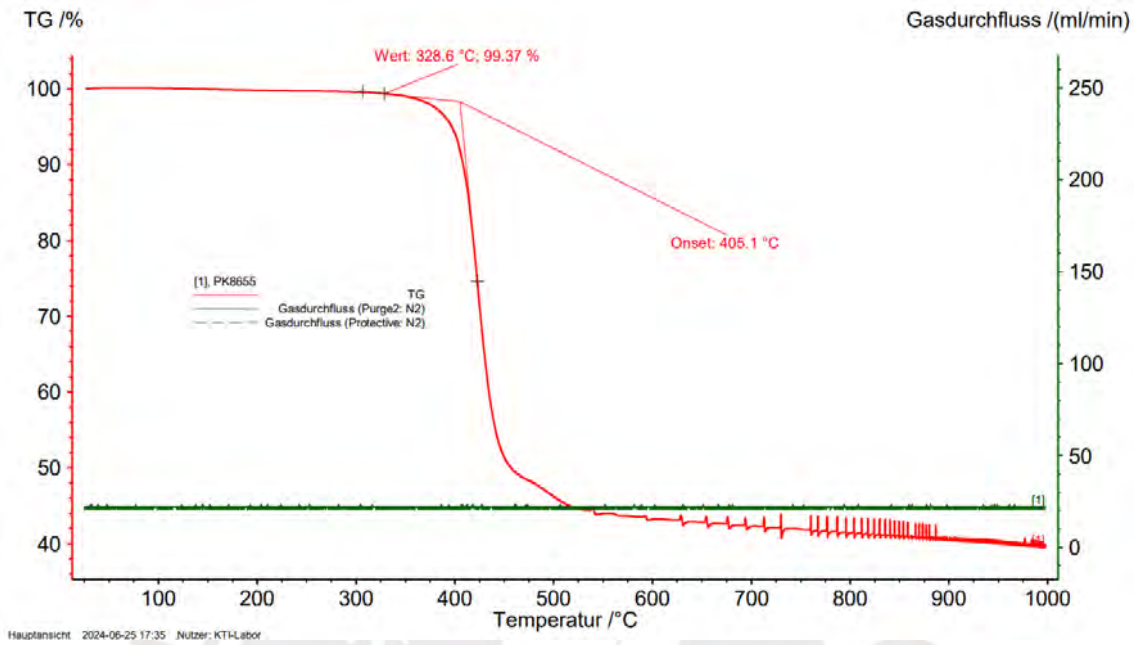

Figure 3.9. TGA thermogram of PK8655 granulates.

3.3 Microstructural comparison of granules PK 6246/8655

Microscope Zeiss AxioScope.A1 instrument was used to analyze the microstructure of both polyketone granules as well as for cross-section analysis after the printing. Figure 3.10 shows microscope Zeiss AxioScope.A1 used for this research.

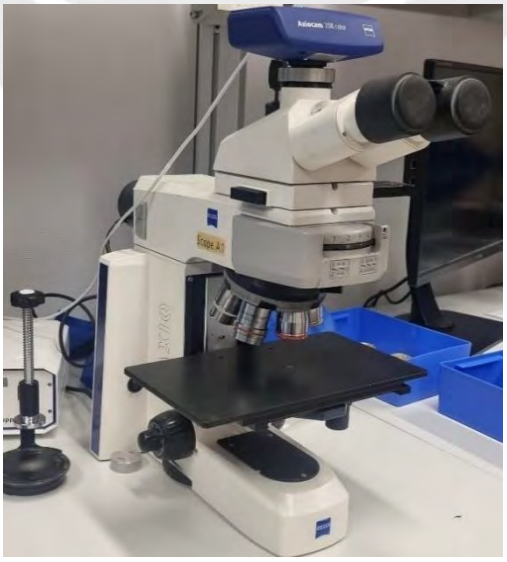

Figure 3.10. Microscope Zeiss AxioScope.A1.

Figure 3.11 and 3.12 show the granulate cross-section of unreinforced polyketone (PK6246) and glass fiber reinforced polyketone (PK8655), respectively. Different oriented glass fibers can be observed on the surface of reinforced polyketone granules. This is presumably due to the arrangement or alignment of the glass fibers.

Figure 3.11. Granule microstructure of PK6246.

Figure 3.12. Granule microstructure of PK8655.

3.4 System specifications

3.4.1 Screw extruder

The customized single screw extruder KE-V 20-25-G from Ematik Gmbh, made in Germany, was assembled for the processing of polyketone. The extruder and motor had

maximum rotational speeds of 100 RPM and 3000 RPM, respectively. The temperature could be set as high as 300 °C with a precision of ±2 °C.

The primary components of the extruder include a hopper with a feed system, a screw, and a nozzle, as illustrated in Figures 3.13 and 3.14. The hopper and feed system are engineered to maintain a steady feeding rate. Before starting the extrusion process, the plasticizing unit (polyketone) was heated for 4 hours at 80°C to reduce humidity according to the recommendations of the supplier (*AKROTEK PK-HM 8 Black (6246).*, n.d.; *AKROTEK PK-VM GF 30 Black (8655).*, n.d.). Then, the plasticizing unit was exposed to five different temperature zones. According to the recommendations of the supplier (*AKROTEK PK-HM 8 Black (6246).*, n.d.; *AKROTEK PK-VM GF 30 Black (8655).*, n.d.), the plasticizing unit must be heated in a range of 220-250 °C in zone 1, zone 2 and zone 3 as shown in Figure 3.13, while in zone 4 and zone 5 in a range of 230-250 °C as shown in Figure 3.14.

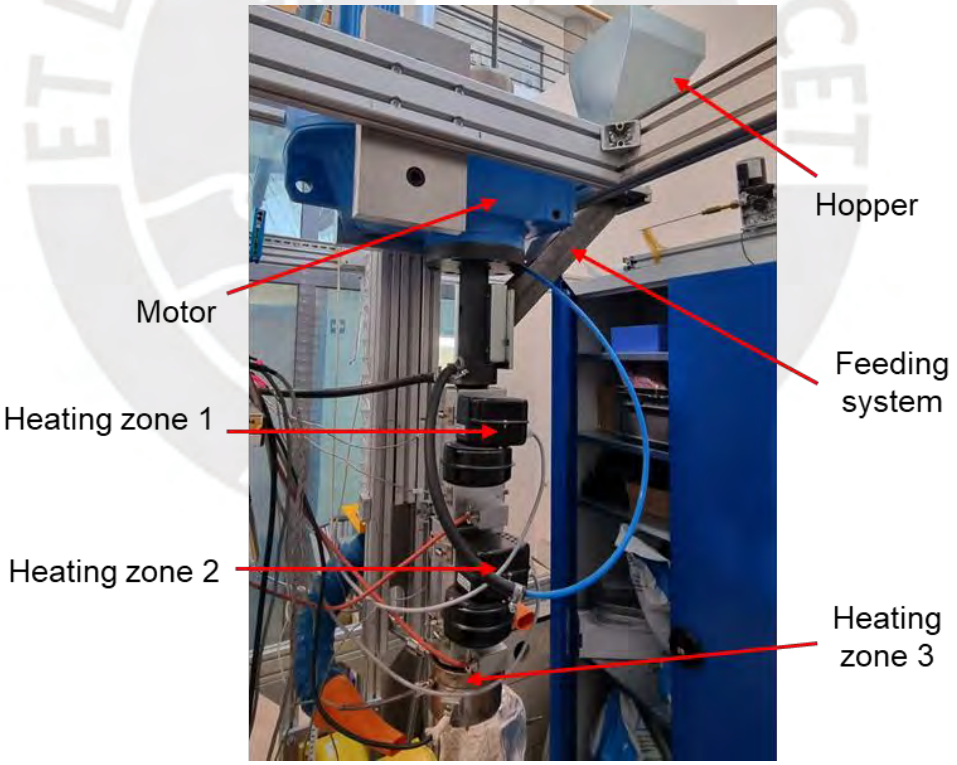

Figure 3.13. Main elements and heating zones of customized screw extruder.

However, during the preliminary tests, it was found that temperatures lower than 220° were required in the first 2 zones of extrusion so that the polyketone in plasticizing unit

does not degrade (this will be explained in more detail in the preliminary tests (Section 4)). While temperatures higher than 220°C were required in the zones 3 and 4 of extruder to obtain a melting of the polyketone. Initially, there was no heating element in zone 5, but it was observed that without heating of the nozzle on exits the polyketone solidified due to the rapid cooling at the exit from the nozzle. As a result, an extra heating element was installed in zone 5 near the nozzle to guarantee the uninterrupted flow of the molten material.

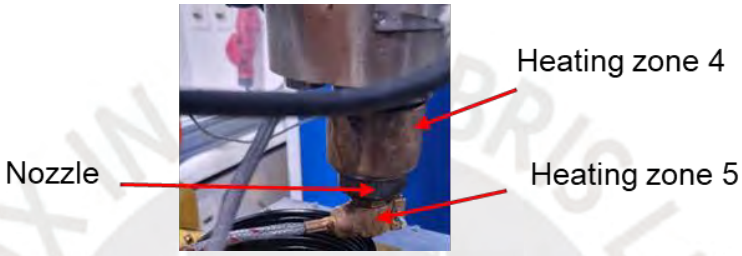

Figure 3.14. Nozzle and heating zones of customized screw extruder.

All temperatures (according to preliminary tests explained in section 4) were kept constant throughout the experimental trials. The nozzle had a diameter of 4 mm, chosen based on prior research indicating that, with the current setup and no additional cooling, this diameter was the largest capable of producing parts with consistent geometry.

3.4.2 Building table

Fanuc Robot LR Mate 200iB with 6 axes, assembled with a building table (240 × 330 mm), was used for the manufacturing of polyketone parts as shown in Figure 3.15. This table incorporates an integrated heating system capable of reaching temperatures up to 200 °C. In experimental tests, the table temperature was adjusted to 200 °C to mitigate the rapid cooling of molten polyketone when it comes into contact with the colder table surface. Furthermore, a single strip of polyimide tape was placed on the upper surface of the table to improve adhesion between the workpiece and the build table.

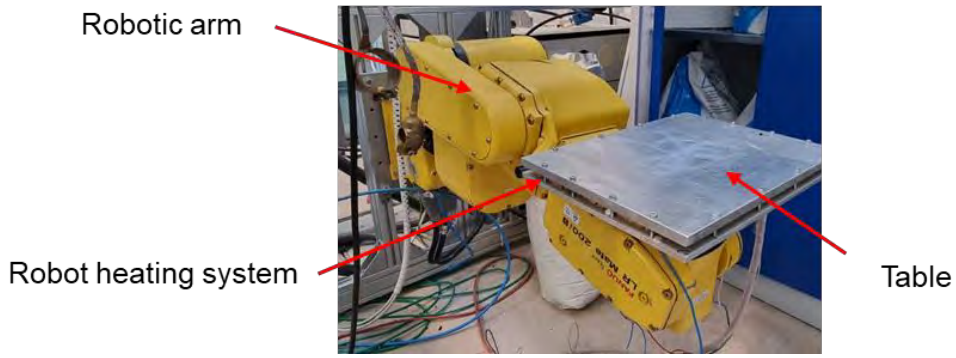

Figure 3.15. Robotic arm assembled with a building table.

The system was configured to manufacture a cylindrical workpiece measuring 140 mm in diameter and 75 mm in height (these dimensions are justified in section 4). Figure 3.16 shows the 3D model that needs to be printed.

Figure 3.16. 3D model of cylindrical workpiece.

Furthermore, the formation of the polyketone pieces was handled by the robotic arm controller as shown in Figure 3.17. In addition, temperature monitoring during the process was carried out using an Optris PI450 model infrared camera, with an emissivity set at 0.9. The camera operates within a temperature range of -20 to 900°C with an accuracy of ±2°C. Thermocouples were used to calibrate thermal emissivity. Thermograms provided the interpass temperatures and line temperatures along the printed part. Measurements were taken at three different locations with a 5 mm gap between each pair of strands for interpass temperatures and at the midpoint of each strand for line temperatures.

Figure 3.17. Robotic arm controller.

3.5 Sample characterization

Following the processing of the workpieces, a thorough characterization was conducted. First, a visual inspection of all printed polyketone parts was performed using a Nikon D5600 DSLR camera. Materialography was then performed with a Zeiss Axio Zoom V16 optical microscope as shown in figure 3.18. To do this, all printed polyketone parts were cut, mounted in Epoxi Resin and polished with abrasive paper (grit 360 to 4800).

Figure 3.18. Microscope Zeiss Axio Zoom V16.

Finally, microhardness and tensile tests were performed to analyze the mechanical properties of polyketone manufactured workpieces. Microhardness testing was conducted by using the standard Vickers microhardness method with Struers DuraScan

70mashine as shown in figure 3.19. The tests were repeated five times for each sample with the HV 0,1 method and the standard deviation was computed.

Figure 3.19. Microhardness machine Struers DuraScan 70mashine.

A Hegewald & Peschke Inspect Retrofit universal testing machine with a maximum load of 20 kN and travel speed of 20 mm/min was used to evaluate tensile properties as shown in figure 3.20.

Figure 3.20. Tensile testing machine Hegewald & Peschke Inspect Retrofit.

The specimens had prismatic shapes with dimensions (height x width x length) 20 x 6 x 75 mm as shown in Figure 3.21.

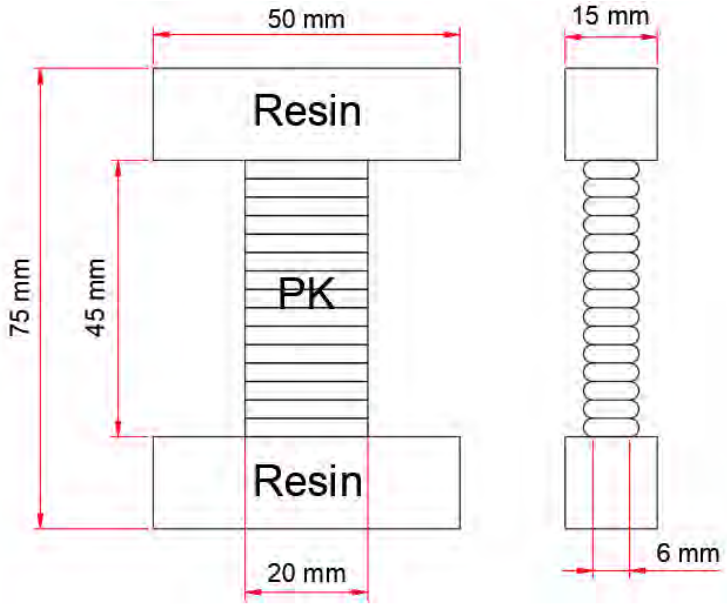

Figure 3.21. Sketch of the samples for tensile testing.

Chapter IV: Preliminary research

4.1 Determination of optimal process parameters

Due the system was programmed to create cylindrical workpieces, it was necessary to determine and delimit certain manufacturing parameters. Some of these parameters were previously defined, which are the following:

- ✓ Building table temperature: 200 °C
- ✓ Workpiece height: 75 mm

As explained in the previous section, the temperature of the build table was set to 200°C to reduce the rapid cooling of the molten polyketone in contact with the table which causes high deformation of the first strand. Likewise, a height of 75 mm was defined for the workpiece since it is a sufficient length to carry out all necessary sample characterization.

However, it was necessary to determine the other process parameters through preliminary tests. The parameters to find were the following:

- ✓ Process temperatures: T_1, T_2, T_3, T_4, T_5
- ✓ Workpiece diameter: D
- ✓ Range of table speeds: v

4.1.1 Determination of optimal process temperatures

In line with the recommendations provided by the polyketone supplier (*AKROTEK PK-HM 8 Black (6246).*, n.d.; *AKROTEK PK-VM GF 30 Black (8655).*, n.d.), temperatures between zone 1 and 4 should be between the 220 - 250 °C while the temperature in nozzle zone should be between 230 - 250 °C. These temperature recommendations are for injection molding. Therefore, several samples of polyketone were manufactured by varying the temperatures of the zones (zone 1 - zone 5) until the optimal process temperatures were found, as shown in figure 4.1. It was found that in the first two extruder zones the temperature should be less than 220º, because in these zones the material is

only required to be plasticized, not melted. The material reaches these temperatures due to the friction produced between the base material granules and the extruder screw, which pushes the polyketone granules against the barrel wall. Besides, if the temperatures are higher than 220°C it causes the polyketone to degrade as it leaves the extruder. On the other hand, it was found that the temperature in the nozzle have to be higher than 260º, because this improves the quality of the molten polyketone when it leaves the extruder.

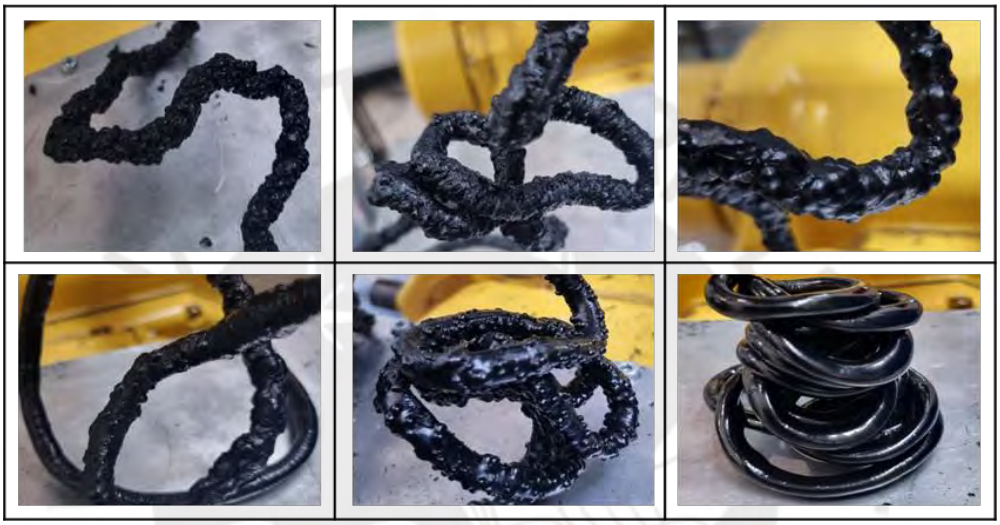

Figure 4.1. Determination of optimal process temperature.

For all these reasons, the optimal temperature parameters were set to be:

- ✓ T_1: 200 °C
- ✓ T_2: 200 °C
- ✓ T_3: 225 °C
- ✓ T_4: 235 °C
- ✓ T_5: 265 °C

4.1.2 Determination of the optimal part diameter

To print cylindrical parts, the optimal diameter must be determined considering the dimensions of the robot table (240 x 330 mm). Therefore, workpieces were manufactured in the range of 50 - 80 mm, with an interval of 10 mm as shown in figure 4.2. These parts

were printed with a table speed of 10 mm/s and the optimal diameter found for printing of cylindrical workpieces was 140 mm. On the one hand, it was observed that with diameters less than 140 mm the workpieces were unstable due to geometric deformations due to high heat accumulation. On the other hand, for diameters greater than 140 mm, the printing height of the workpiece could not be reached due to the dimensional restrictions of the robotic arm.

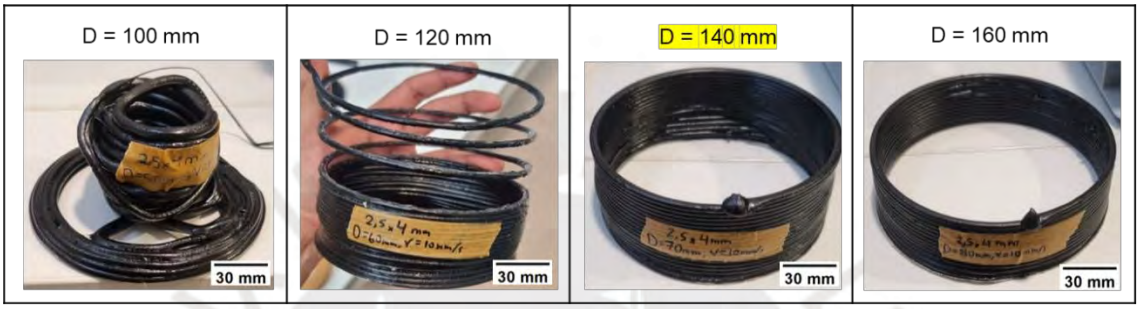

Figure 4.2. Determination of the optimal workpiece diameter.

4.1.3 Determination of optimal range of table speeds

Due to the wide number of possible table speeds, the speed must be limited before starting the tests. Therefore, cylindrical parts were printed in a table speed range of 5 - 20 mm/s with an interval of 5 mm/s as shown in figure 4.3. These parts were printed with a diameter of 140 mm.

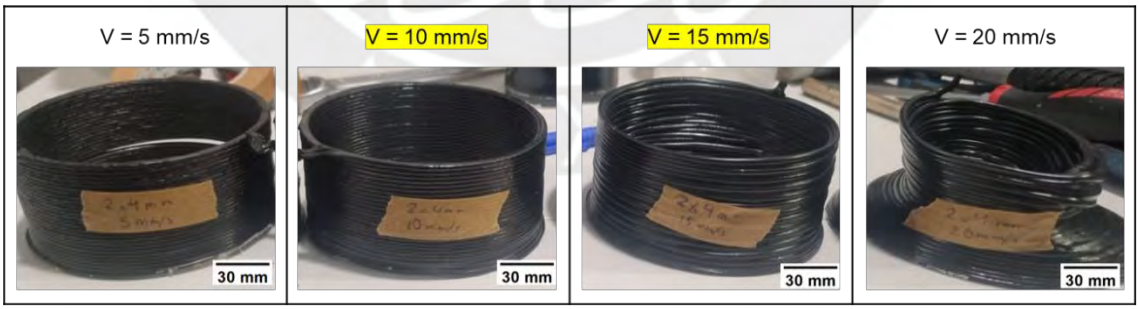

Figure 4.3. Determination of optimal range of table speeds.

It could be observed that at very low table speeds, such as 5 mm/s, the material began to degrade. Therefore, it is not an appropriate speed for the manufacture of cylindrical polyketone workpieces. On the other hand, at very high table speeds, such as 20 mm/s,

the workpiece began to deform due to the excess accumulated heat. Therefore, it is not an optimal speed for the manufacture of cylindrical polyketone workpieces either.

Finally, optimal results were obtained with table speeds of 10 and 15 mm/s. Therefore, both speeds were used in the final experiments.

4.2 Mathematical model of strand deposition

A strand deposition model was proposed by Schmidt et al. (2019). This model describes the geometry of the strand (height and width) as a function of the rotation speed of extruder and the travel speed of robot arm. Figure 4.4 illustrates the strand geometry of the cylindrical workpieces to be printed.

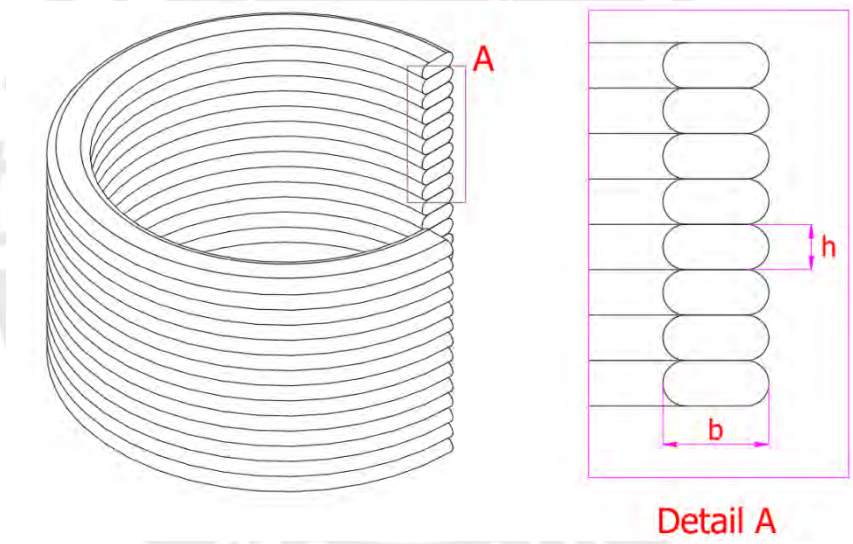

Figure 4.4. Representation of strand geometry of the cylindrical workpieces.

A strand deposition model was formulated under the assumption that the mass and volumetric flow rates inside and outside the extruder are balanced, taking into account the constant density of the polyketone in both the solid and molten states. According to the principle of conservation of mass, it is defined:

$$\dot{m}_i = \dot{m}_o \tag{1.1}$$

$$k_{mat} = \frac{\Delta \dot{m}_i}{\Delta n_i} \tag{1.2}$$

$$\dot{m}_i = n_i \cdot k_{mat} \tag{1.3}$$

n_i: Extruder speed

k_{mat}: Material constant (slope of the curve)

$\dot{m}_i$: Mass flow inside the extruder

$\dot{m}_o$: Mass flow outside the extruder

Likewise, according to the principle of conservation of volume and considering a constant density of the material, it is defined:

$$\dot{V}_i = \dot{V}_o \tag{1.4}$$

$$\rho = \frac{m}{V} \rightarrow \dot{V} = \frac{\dot{m}}{\rho} \tag{1.5}$$

ρ : Density

$\dot{V}_i$: Volume flow inside the extruder

$\dot{V}_o$: Volume flow outside the extruder

Replacing equation 1.3 into 1.5, its obtained:

$$\dot{V}_o = n_i \cdot k_{mat} \cdot \frac{1}{\rho} \tag{1.6}$$

Furthermore, the volume flow inside and outside the extruder can be described as a function of the geometry of strand (Figure 4.5) and the speed of the robotic arm.

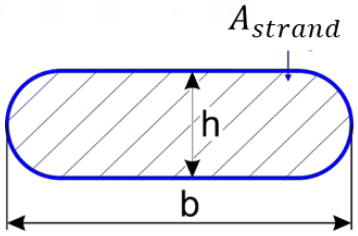

Figure 4.5. Sketch of strand geometry.

According to figure 4.5, the area of the strand is described as:

$$A_{Strand} = \left(\frac{\pi}{4} \cdot h^2 + h \cdot (b - h)\right) \quad (1.7)$$

A_{strand}: Area of strand
h: Strand height
b: Strand width

Thus, the volume flow of the extruder is described as:

$$\dot{V}_i = \dot{V}_o = A_{Strand} \cdot v_r \quad (1.8)$$

Replacing equation 1.7 into 1.8, its obtained:

$$\boldsymbol{\dot{V}_o = \left(\frac{\pi}{4} \cdot h^2 + h \cdot (b - h)\right) \cdot v_r} \quad (1.9)$$

v_r: Robot table speed

Finally, by equating equations 1.6 and 1.9, the rotational speed of the extruder and the table speed of the robot were determined.

$$\dot{V}_o = n_i \cdot k_{mat} \cdot \frac{1}{\rho} = (A_{Strand}) \cdot v_r \quad (2.0)$$

- Determination of extruder rotational speed:

$$\boldsymbol{n_i = A \cdot v_r \cdot \frac{1}{k_{mat}} \cdot \rho \ [RPM]} \quad (2.1)$$

- Determination of robot table speed:

$$\boldsymbol{v_R = \frac{1}{A} \cdot n_i \cdot k_{mat} \cdot \rho \ \left[\frac{mm}{s}\right]} \quad (2.2)$$

4.3 Estimation of the material constant

Material constant (K_{mat}) is a constant established through experimental determination. For that purpose, 10 samples of each type of material were printed using an extruder rotation speed from 10 to 100 rpm, increasing in an interval of 10 rpm. All samples were measured after an interval of 60 s of printing and all measurements were repeated three times for more accurate results. A digital precision balance Kern PLJ was used to weigh each sample as shown in Figure 4.6.

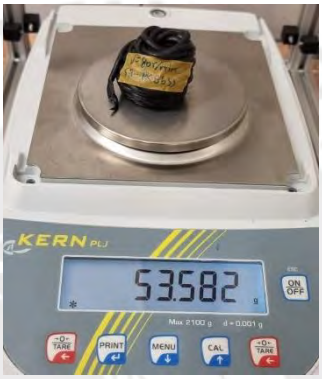

Figure 4.6. Digital precision balance Kern PLJ.

The results obtained from both polyketone materials (PK6246 and PK8655) are shown in Figure 4.7. Characteristic curves show a direct relationship between applied extruder rotational speed and measured mass output, and the slope of each characteristic curve represents the material constant.

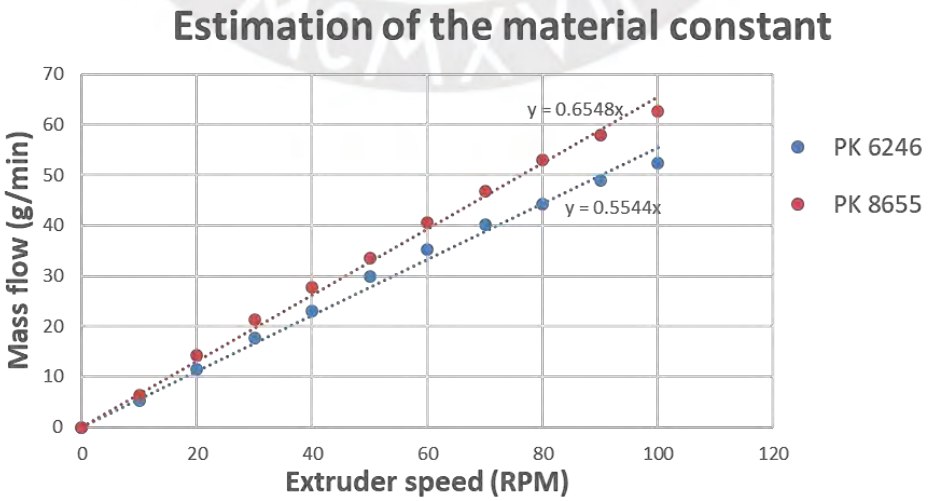

Figure 4.7. Characteristic curves for estimation of material constant.

4.4 Printing process window – Strand height and width

Material constant (K_{mat}) was added in equations 2.1 and 2.2 from section 4.2 to determine the process parameters. For the correct choice of width (b) and height (h) of the strand, the mass flow of each material was considered.

The strand height was set within the range of 1.5 to 3.5 mm (1.5, 2.0, 2.5, 3.0 and 3.5 mm). This occurs because when the strand height is less than 1.5 mm, the material cools too quickly, causing the initial strand to bend. This bending results in a collision between the nozzle and the first strand during the deposition of the second strand. Furthermore, a 4 mm nozzle diameter restricts the maximum theoretical value of the strand height to 4 mm. Therefore, a maximum strand height value of 3.5 mm is chosen, since the theoretical maximum value of 4mm is not achievable.

On the other hand, the strand width was configured to be 4.0, 5.0 and 6.0 mm. The minimum strand width of 4 mm was limited by the nozzle diameter, while strand widths exceeding 6 mm resulted in significant geometry deviations and a significant increase in porosity of workpieces. To achieve larger strand widths, a nozzle with a bigger diameter should be utilized.

Finally, the travel speed of the build table was configured to be 10 and 15 mm/s, according to preliminary experiments in section 4.1.3. Thus, thirty workpieces of both materials were printed following the parameters shown in table 4.1.

Table 4.1. Printing process window – Strand height and width.

PK6246/8655															
Table speed (mm/s)	Serie (width) 4 mm					Serie (width) 5mm					Serie (width) 6mm				
	Strand height (mm)					Strand height (mm)					Strand height (mm)				
	1.5	2.0	2.5	3.0	3.5	1.5	2.0	2.5	3.0	3.5	1.5	2.0	2.5	3.0	3.5
10															
15															

According to the model shown in section 4.2, the ratios between extruder rotational speed, table speed and strand were calculated. Figures 4.8, 4.9 and 4.10 show the relationships between extruder speed and strand height for strand widths of 4, 5 and 6 mm respectively.

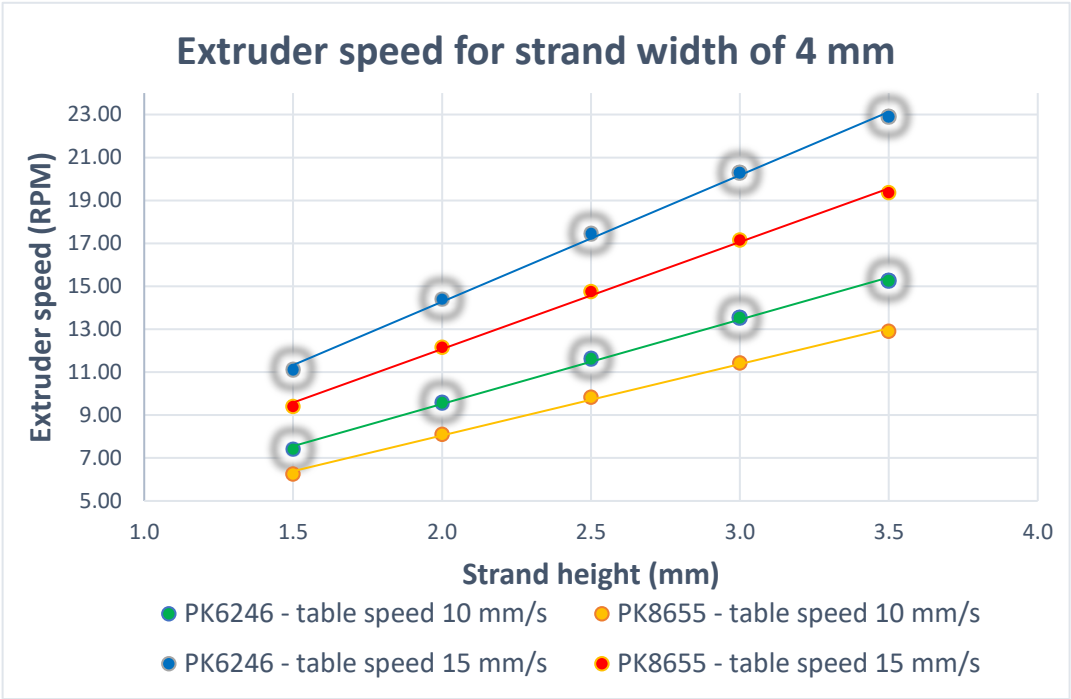

Figure 4.8. Extruder speeds for strand width of 4 mm.

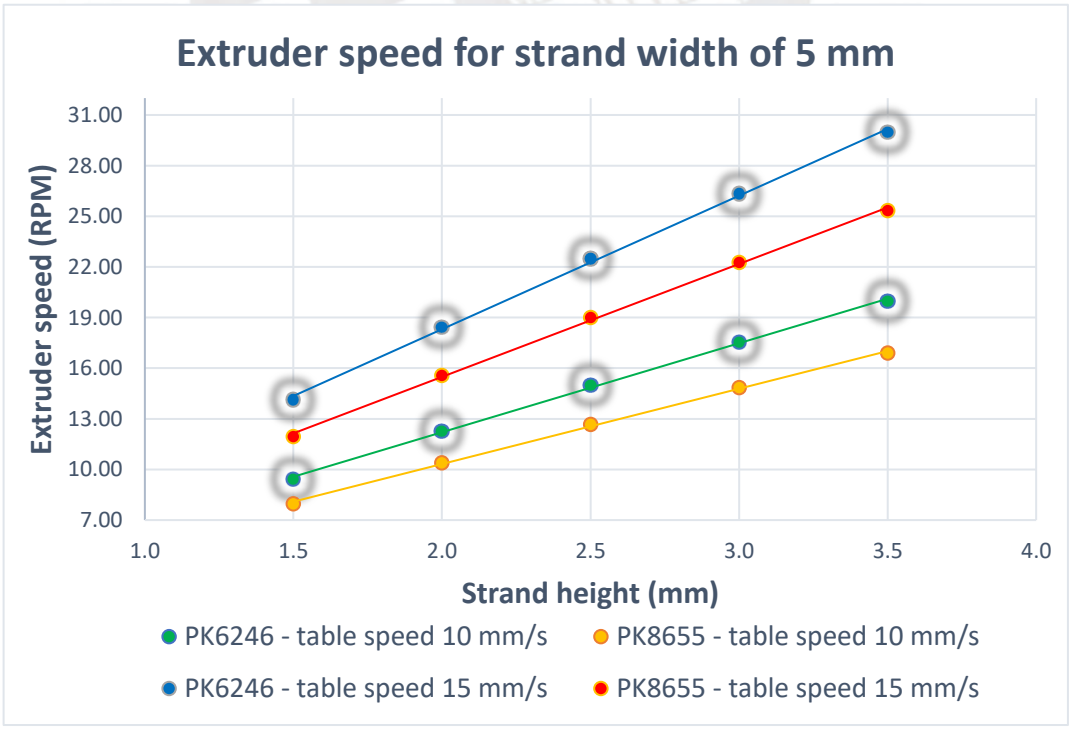

Figure 4.9. Extruder speeds for strand width of 5 mm.

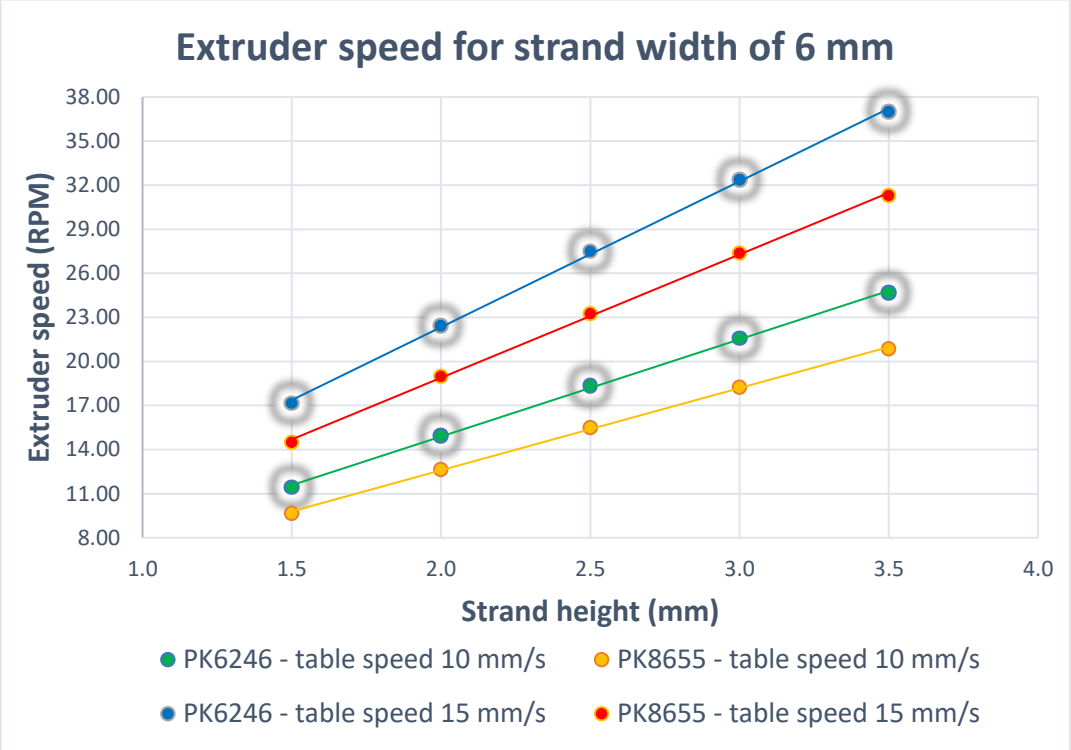

Figure 4.10. Extruder speeds for strand width of 6 mm.

From graphs 4.5, 4.6 and 4.7 shown, a direct relationship can be observed between the rotational speed of the extruder and the height of the strand. In addition, higher extrusion speeds were observed for the PK6246 material than for the PK8655 material at the same printing conditions. Finally, the other printing parameters of the polyketones PK6246 and PK8655 were determined and arranged in tables 4.2 and 4.3 respectively.

Table 4.2. Printing parameters of PK6246 material.

ID-Number	Strand height [mm]	Strand width [mm]	Strand area [mm^2]	Table speed [mm/s]	Extruder speed [RPM]	Motor speed [RPM]	Table [°C]
10.1.5.4	1.5	4.0	5.52	10	7.41	148	200
10.2.4	2.0	4.0	7.14	10	9.59	192	200
10.2.5.4	2.5	4.0	8.66	10	11.63	233	200
10.3.4	3.0	4.0	10.07	10	13.52	270	200
10.3.5.4	3.5	4.0	11.37	10	15.27	305	200
15.1.5.4	1.5	4.0	5.52	15	11.11	222	200
15.2.4	2.0	4.0	7.14	15	14.39	288	200
15.2.5.4	2.5	4.0	8.66	15	17.44	349	200
15.3.4	3.0	4.0	10.07	15	20.28	406	200
15.3.5.4	3.5	4.0	11.37	15	22.91	458	200
10.1.5.5	1.5	5.0	7.02	10	9.42	188	200
10.2.5	2.0	5.0	9.14	10	12.28	246	200
10.2.5.5	2.5	5.0	11.16	10	14.99	300	200
10.3.5	3.0	5.0	13.07	10	17.55	351	200
10.3.5.5	3.5	5.0	14.87	10	19.97	399	200
15.1.5.5	1.5	5.0	7.02	15	14.14	283	200
15.2.5	2.0	5.0	9.14	15	18.42	368	200
15.2.5.5	2.5	5.0	11.16	15	22.48	450	200
15.3.5	3.0	5.0	13.07	15	26.33	527	200
15.3.5.5	3.5	5.0	14.87	15	29.96	599	200
10.1.5.6	1.5	6.0	8.52	10	11.44	229	200
10.2.6	2.0	6.0	11.14	10	14.96	299	200
10.2.5.6	2.5	6.0	13.66	10	18.34	367	200
10.3.6	3.0	6.0	16.07	10	21.58	432	200
10.3.5.6	3.5	6.0	18.37	10	24.67	493	200
15.1.5.6	1.5	6.0	8.52	15	17.16	343	200
15.2.6	2.0	6.0	11.14	15	22.44	449	200
15.2.5.6	2.5	6.0	13.66	15	27.51	550	200
15.3.6	3.0	6.0	16.07	15	32.37	647	200
15.3.5.6	3.5	6.0	18.37	15	37.01	740	200

Table 4.3. Printing parameters of PK8655 material.

ID-Number	Strand height [mm]	Strand width [mm]	Strand area [mm^2]	Table speed [mm/s]	Extruder speed [RPM]	Motor speed [RPM]	Table [°C]
10.1.5.4	1.5	4.0	5.52	10	6.27	125	200
10.2.4	2.0	4.0	7.14	10	8.11	162	200
10.2.5.4	2.5	4.0	8.66	10	9.84	197	200
10.3.4	3.0	4.0	10.07	10	11.44	229	200
10.3.5.4	3.5	4.0	11.37	10	12.92	258	200
15.1.5.4	1.5	4.0	5.52	15	9.40	188	200
15.2.4	2.0	4.0	7.14	15	12.17	243	200
15.2.5.4	2.5	4.0	8.66	15	14.75	295	200
15.3.4	3.0	4.0	10.07	15	17.16	343	200
15.3.5.4	3.5	4.0	11.37	15	19.37	387	200
10.1.5.5	1.5	5.0	7.02	10	7.97	159	200
10.2.5	2.0	5.0	9.14	10	10.38	208	200
10.2.5.5	2.5	5.0	11.16	10	12.67	253	200
10.3.5	3.0	5.0	13.07	10	14.84	297	200
10.3.5.5	3.5	5.0	14.87	10	16.89	338	200
15.1.5.5	1.5	5.0	7.02	15	11.96	239	200
15.2.5	2.0	5.0	9.14	15	15.58	312	200
15.2.5.5	2.5	5.0	11.16	15	19.01	380	200
15.3.5	3.0	5.0	13.07	15	22.27	445	200
15.3.5.5	3.5	5.0	14.87	15	25.34	507	200
10.1.5.6	1.5	6.0	8.52	10	9.67	193	200
10.2.6	2.0	6.0	11.14	10	12.66	253	200
10.2.5.6	2.5	6.0	13.66	10	15.51	310	200
10.3.6	3.0	6.0	16.07	10	18.25	365	200
10.3.5.6	3.5	6.0	18.37	10	20.87	417	200
15.1.5.6	1.5	6.0	8.52	15	14.51	290	200
15.2.6	2.0	6.0	11.14	15	18.98	380	200
15.2.5.6	2.5	6.0	13.66	15	23.27	465	200
15.3.6	3.0	6.0	16.07	15	27.38	548	200
15.3.5.6	3.5	6.0	18.37	15	31.30	626	200

Chapter V: Results and discussions

5.1 Geometrical deviation

During the extrusion process, it was observed that the geometric stability depends on the process parameters (Table 4.2 and Table 4.3) and the type of material.

Figures 5.1 and 5.2 show the workpieces from PK6246 and PK8655 produced according to the established parameters (strand width, strand height and table speed).

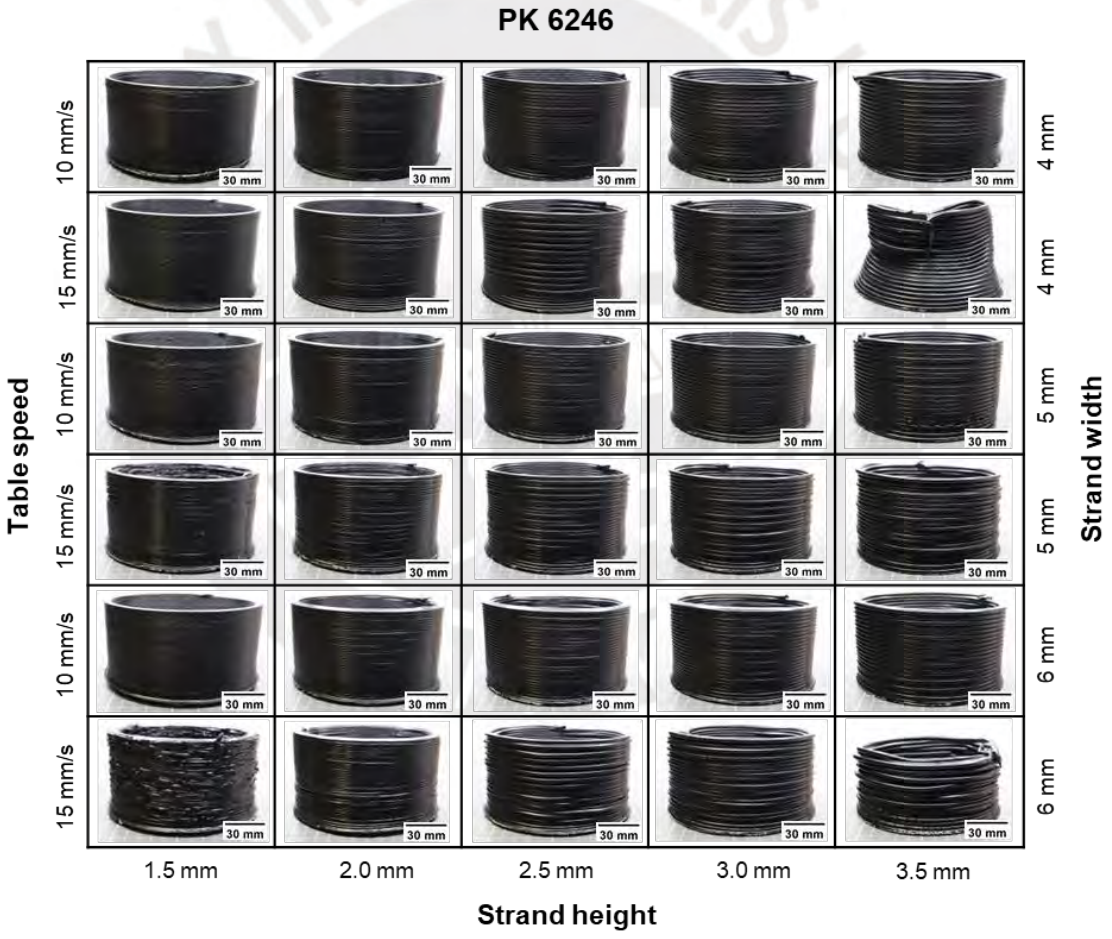

Figure 5.1. Printed workpieces from PK6246.

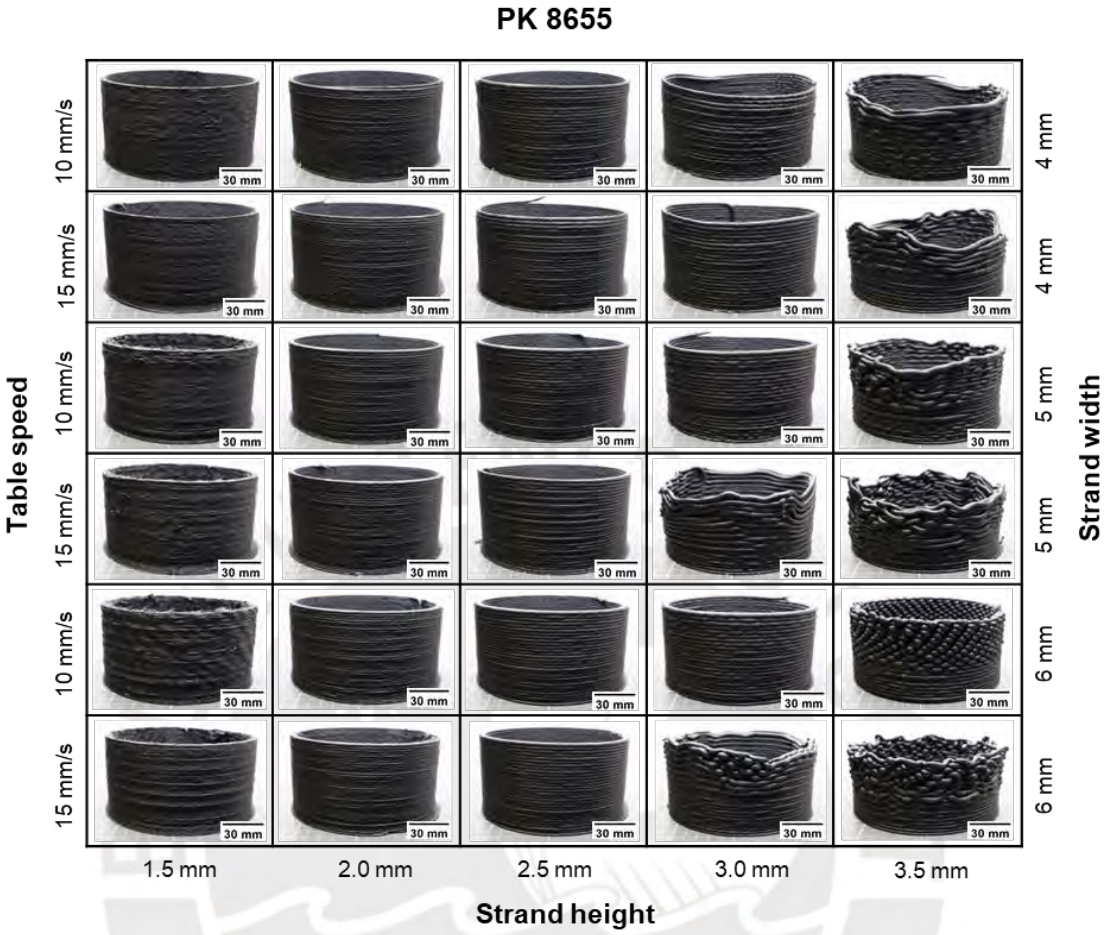

Figure 5.2. Printed workpieces from PK8655.

Firstly, the influence of the table speed had an effect related with the deformation of the workpieces, due to the accumulation of heat in the strands. This heat accumulation caused sinking, mainly in workpieces with strand heights of 3.0 and 3.5 mm, due to the short cooling time from when a strand was deposited to the deposition of the next strand. Second, the strand width also had an effect on the deformation of the workpieces, The workpieces with a strand width of 4 mm generally had greater geometric stability than the workpieces with a strand width of 6 mm. This was also due to the accumulation of heat between strands, since increasing the width of the strands generates a greater contact area between strands. Finally, the strand height had a particular influence on the geometric stability of the workpiece as shown in Figures 5.3 and 5.4.

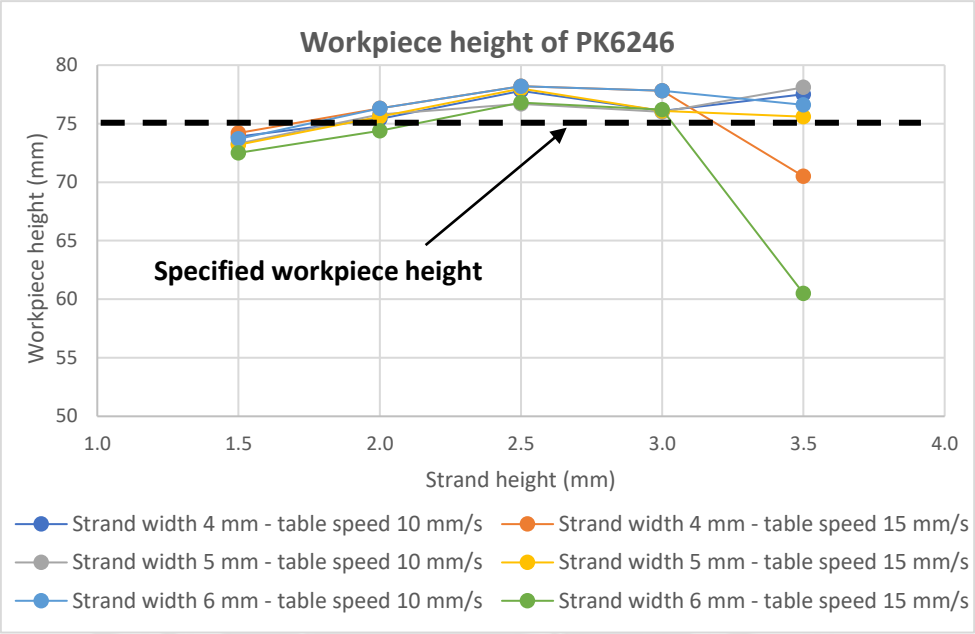

Figure 5.3. Workpiece height of PK6246.

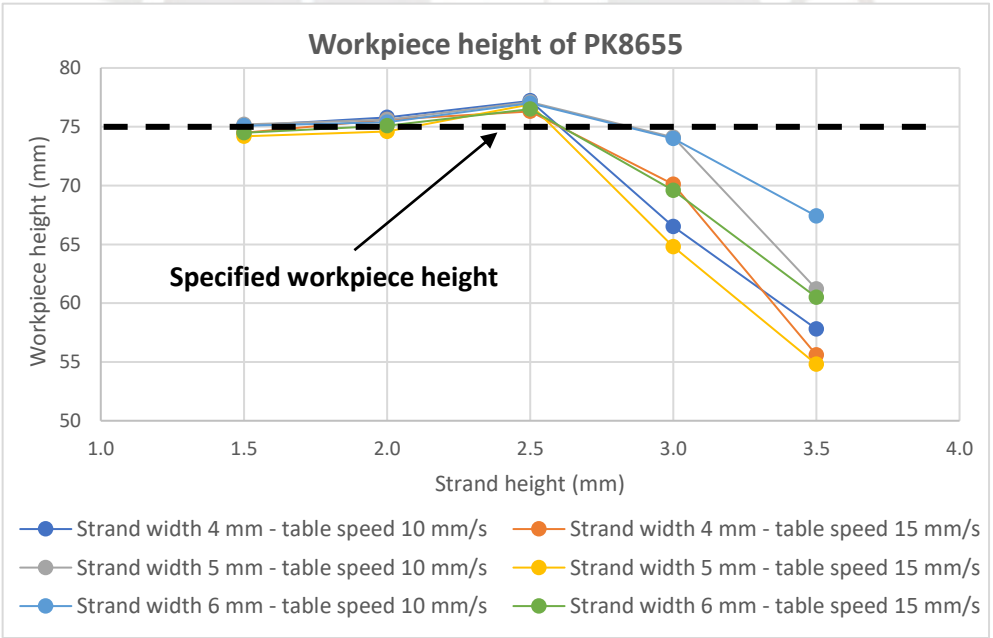

Figure 5.4. Workpiece height of PK8655.

It could be observed that some printed workpieces had a slight increase in height compared to the programmed height. On the one hand, this increase in height occurred because the predefined height depends on the strand height, that is, for example, for a strand height of 2.0 mm, it is not possible to reach the predefined 75 mm height, but rather 76 mm (with 38 strands) will be reached. On the other hand, for example, for

strand heights of 2.5 mm or 3.0 mm, which can both reach the height of 75 mm with 30 and 25 strands respectively, the increase in the final height of workpiece was due to the die-swell effect. That phenomenon occurs when a viscoelastic material (such as a molten polymer) leaves a nozzle and expands to a diameter larger than the nozzle itself. This happens because the material, under pressure within the nozzle, stores elastic energy, which is released as the material exits, causing it to swell (Colon et al., 2023). Factors such as the material's viscoelastic properties, extrusion speed, and nozzle design can influence the degree of swelling. The relevance of the viscoelastic properties of the material was evident in the difference in extruded strand diameter between PK6246 and PK8655. The extruded strand of PK6246 expanded more than that of PK8655.

Another type of geometric deviation was observed in the workpieces (mainly in PK6246) with a strand width of 1.5 mm in which the height of the printed workpiece is slightly less than the programmed height. This happened because the material cooled too quickly, leading to bending of the initial printing strand. The phenomenon responsible for the bending of the first printing strand in additive manufacturing is often referred to as "warping" or "curling". Warping in additive manufacturing refers to the unwanted bending or distortion of a printed part, particularly in the base strands, which can cause the part to lift off the building table or develop a curved, uneven surface (Brion et al., 2022). This phenomenon is most common in thermoplastic materials and there are some factors for this type of deformation. The temperature gradient is one of the main factors since the temperature difference between the extruded material and the outside environment can cause uneven cooling. Besides, during the cooling process, residual stresses can develop within the printed strands due to uneven contraction. These stresses can cause the part to deform and lift from the building table (Stavropoulos et al., 2019). Other relevant factors are poor adhesion to the construction table and its respective temperature.

Furthermore, a dependence between the height of the piece and the height of the strand could be observed, that is, an increase in deformation due to an increase in the height of the strand. According to Schmidt et al. (2019), an increase in the height and width of the strands generates an increase in the application of mass flow. This causes an increase in heat accumulation and consequently high deviation and poor thermal stability. Thus, a notable geometric deviation of 10-25 % was found in workpieces of PK8655 with a strand height of 3.5 mm, while for PK6246 workpieces the geometric

deviation was 5-20 %. This difference in geometric deviation between both materials could be due to the thermal expansion coefficient, crystallinity and mechanical properties.

Finally, although all workpieces printed with PK8655 have a rougher surface than workpieces printed with PK6246, this is because PK8655 is a polyketone reinforced with glass fibers. However, a very poor surface finish could be observed in the workpieces (both materials) with strand height of 1.5 mm and strand width of 6 mm. This occurred because thin strands of printing cause weaker adhesion between strands if the strands are not bonded properly. This can cause delamination and rough surface textures. Moreover, low strand height increases the backpressure in the extruder, which can affect the precision and consistency of the material deposition (Golhin et al., 2023).

5.2 Thermographic analysis

Figures 5.5 and 5.6 illustrate the thermograms taken during the deposition of the final strand just before completing the process.

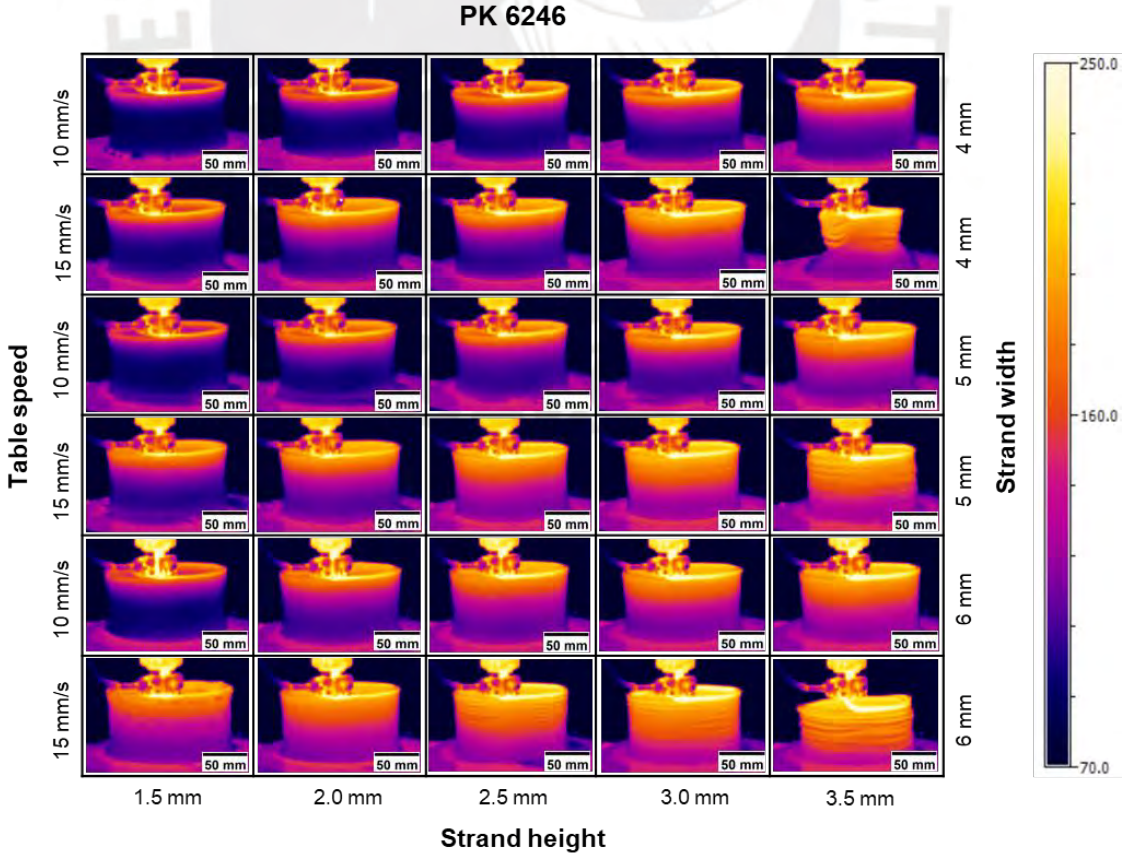

Figure 5.5. Thermograms for all workpieces of PK6246.

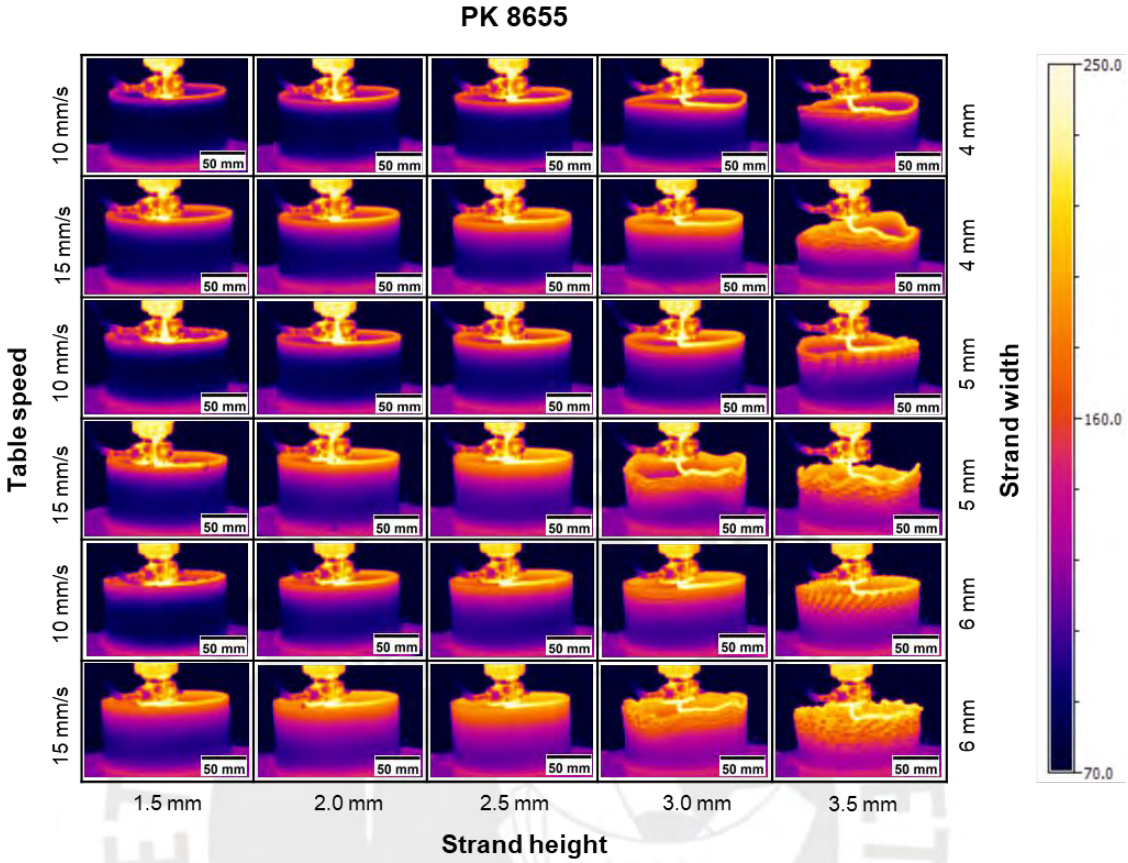

Figure 5.6. Thermograms for all workpieces of PK8655.

Thermograms indicate a clear correlation between temperature distribution, table speed, and strand geometry. With the increase of all these variables, more heat is retained in the workpieces because the lower strands did not have enough cooling time before the next strands were deposited. This high heat accumulation caused some workpieces to deform and sink. Besides, greater deformation could be observed in the PK8655 workpieces than the PK6246 workpieces, despite having less heat accumulation and were manufactured with the same printing parameters. This was possibly due to the different thermal expansion coefficients of both materials. Frieden Templeton et al. (2024) found that controlling the cooling rate and using materials with lower thermal expansion coefficients can significantly reduce shrinkage and warpage.

On the other hand, during the printing of the first strands, the heating of the table had a great influence on reducing the rapid cooling of the strands in contact with the table. This is mainly important for workpieces printed with a strand width of 4 mm to avoid warping. Thesiya & Lepsik et al. (2023) concluded that warping and residual stresses in FDM parts

are primarily due to thermal gradients during the cooling process. Thus, it´s recommended optimizing the cooling rate and modifying the build environment to reduce thermal stresses.

Furthermore, strand height also had an influence on heat accumulation and workpiece sinking. Figures 5.7 and 5.8 illustrate the interpass temperatures at the moment before the next strand is deposited. For this, the series with a strand width of 5 mm was chosen for both materials and the temperature was recorded in each strand. A clear relationship was observed between the height of the strand and the interpass temperature, that is, a greater height of the strand increases the interpass temperature. The maximum and minimum interpass temperature of PK6246 was ~195°C and ~165 °C respectively, while for PK8655 it was ~185 °C and ~150 °C. These maximum and minimum temperatures were related to the deformation of the printed work pieces, since a greater accumulation of heat generates greater sinking of the material due to the pressure of the piece's own weight. Another important aspect that was observed was a lower interpass temperatures during the printing of the first strands. Workpieces with a strand height of 1.5 mm were the most sensitive to warping due to rapid cooling. This is related to the geometric deviation due to warping of the workpieces seen in section 5.1.

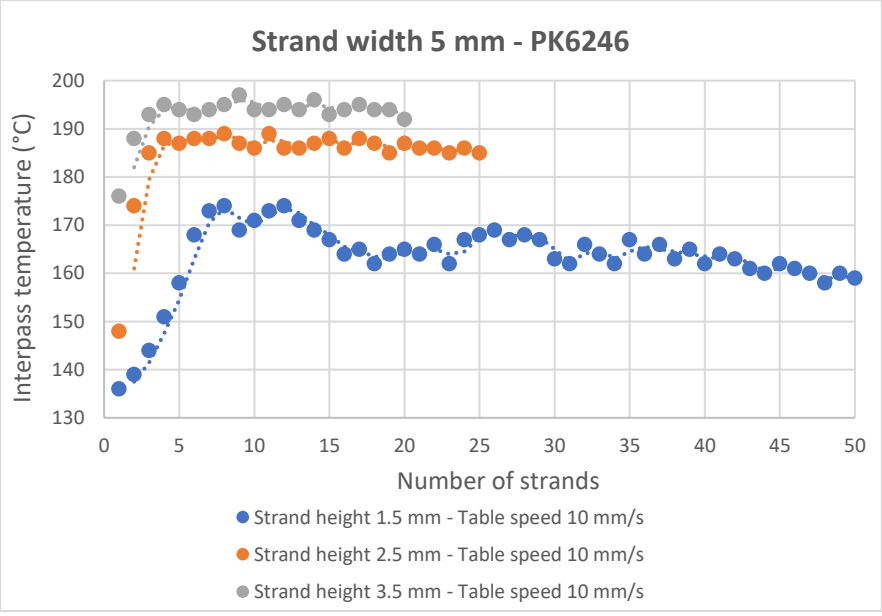

Figure 5.7. Interpass temperatures for different strand heights of PK6246.

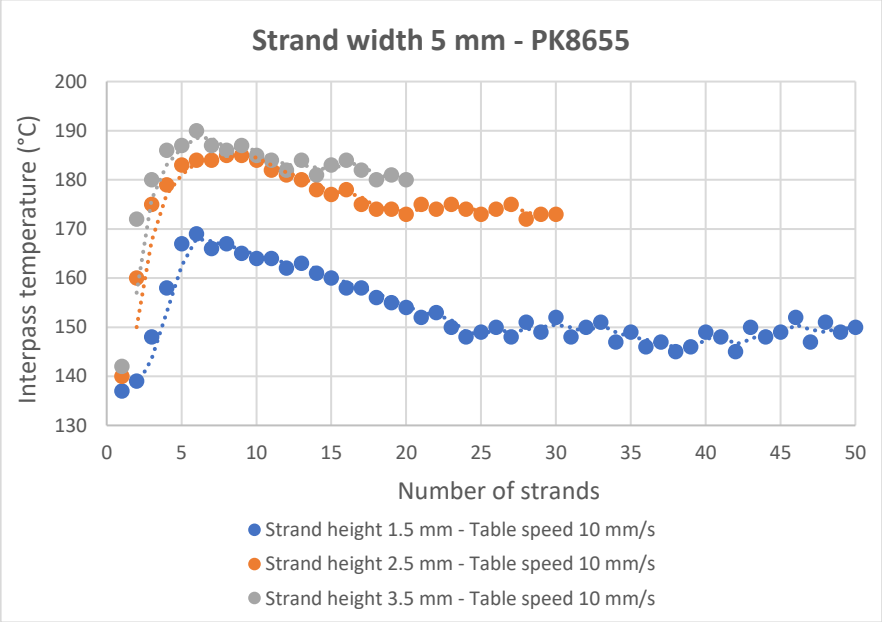

Figure 5.8. Interpass temperatures for different strand heights of PK8655.

Finally, the table speed during the printing process also affects interpass temperatures. Figures 5.9 and 5.10 illustrate the interpass temperatures at the moment before the next strand is deposited for table speeds of 10 mm/s and 15 mm/s. For this, the series with a strand width of 4 mm was chosen for both materials and the temperature was recorded in each strand. It could be observed that with the increase in the speed of table speed (build table), interpass temperatures increase as well. The interpass temperature in a PK6246 workpiece printed at a travel speed of 10 mm/s was approximately 185 °C, whereas at 15 mm/s it was around 195 °C. Similarly, the interpass temperature in a PK8655 workpiece printed at 10 mm/s was about 175 °C, compared to roughly 185 °C at 15 mm/s. This slight difference between temperature ranges is presumably due the thermal properties of the materials.

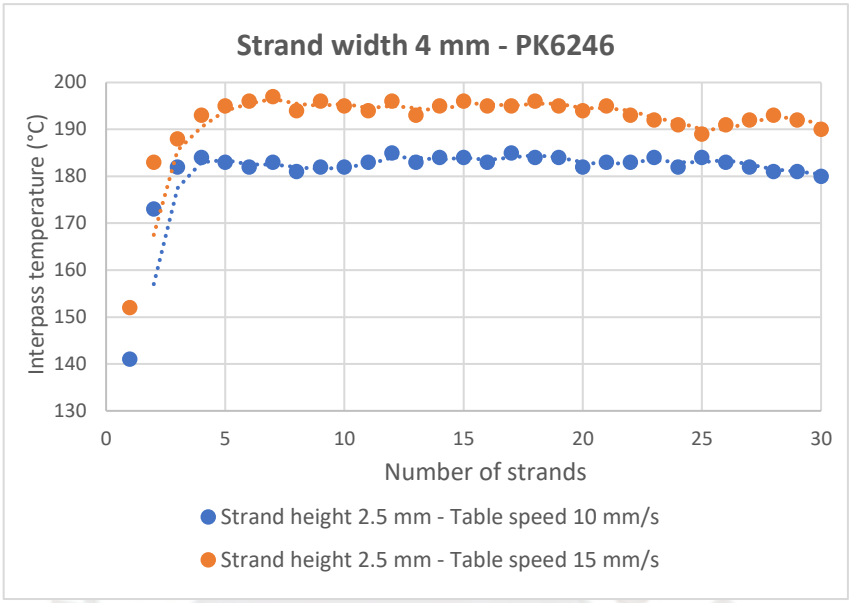

Figure 5.9. Interpass temperatures for different table speeds of PK6246.

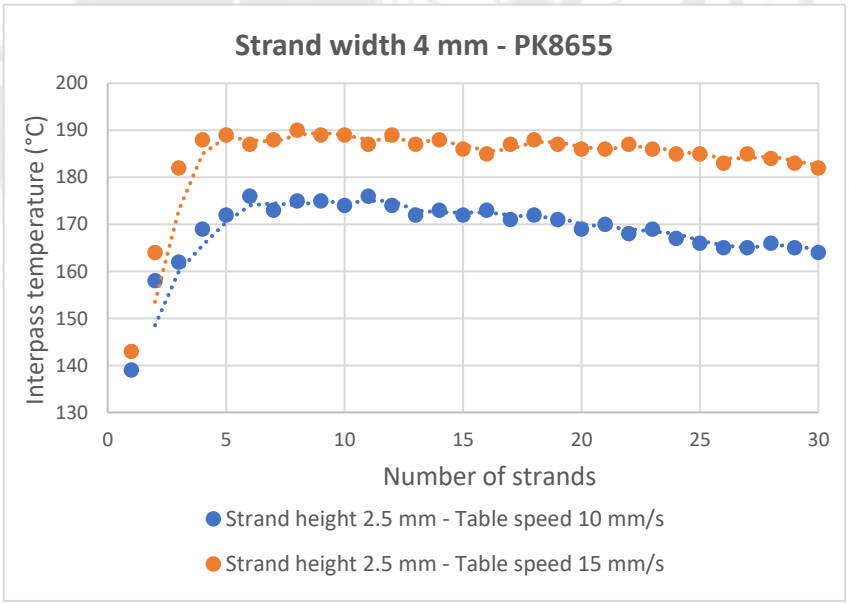

Figure 5.10. Interpass temperatures for different table speeds of PK8655.

5.3 Mechanical properties

To analyze how process parameters influence the quality of the printed parts, mechanical properties such as hardness and tensile strength were assessed through testing.

5.3.1 Hardness test

Figure 5.11 shows the results of hardness tests results for both materials (PK6246 and PK8655). The samples for these tests were obtained from workpieces with strand heights of 1.5 and 3.5 mm. Likewise, the granules of the base material were also evaluated.

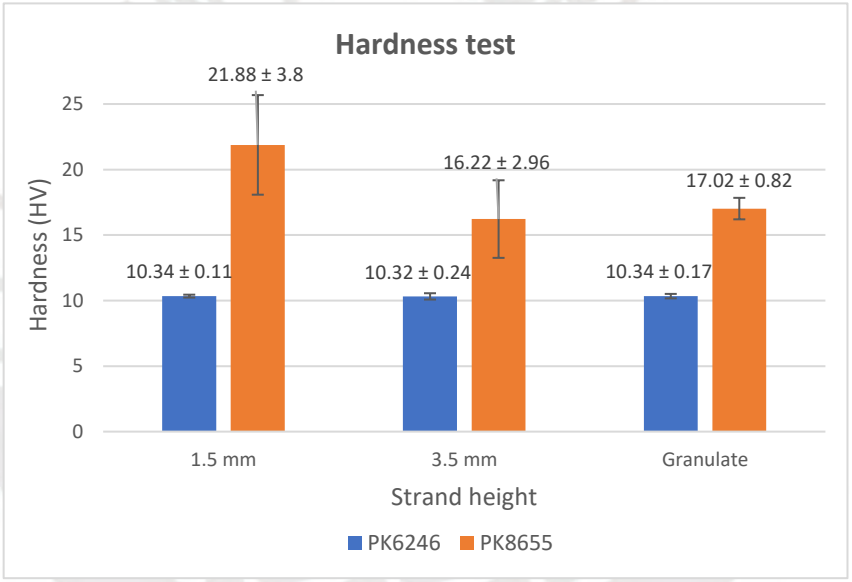

Figure 5.11. Hardness test for PK6246 and PK8655.

The results obtained from the PK6246 material were similar with a value of ~10.34 ± 0.17 HV. However, the results of the PK8655 material do not present the same similarity in values. The PK8655 sample with a strand height of 1.5 mm presented a hardness of 21.88 ± 3.8 HV, while the other samples of PK8655 presented a hardness value of ~16.42 ± 2.3 HV. This could be due to the arrangement of the glass fibers in the PK8655 material.

On the other hand, all the PK8655 samples showed a higher Vickers hardness with respect to the PK6246 samples. This is because the PK8655 material is a polyketone reinforced with glass fibers. This difference in hardness can also be verified in the

mechanical properties given by the supplier. George Wypych et al. (2016) concluded that the addition of fillers (e.g., glass fibers) and plasticizers can significantly alter the hardness of polymers. Fillers generally increase hardness, while plasticizers decrease it by increasing flexibility.

5.3.2 Tensile test

Figures 5.12 illustrates the tensile test results (Inter-road bond strengths) for all printed workpieces (PK6246 and PK8655). All tensile tests were carried out with a rater angle of 90° and each test was repeated 5 times to have more precise values. Inter-road bond strength of samples obtained was highly influenced by the process parameters and interpass temperature.

A considerable difference in inter-road bond strength could be noticed between the PK6246 and PK8655 samples, despite the fact that they were manufactured under the same printing parameters. This was mainly due to the properties of each type of material. Chancon et al. claims that different polymers exhibit varying levels of inter-road bond strength due to their inherent material properties. For instance, polymers with higher viscosities or lower melt flow indices tend to form stronger inter-road bonds due to better flow and wetting characteristics during the printing process (Chacón et al., 2017).

The highest inter-road bond strength for PK6246 was 42.4 ± 5.2 MPa and it was obtained in the sample printed with strand width × height of 5.0 × 2.0 mm and table speed of 10 mm/s. This value is ~ 70% of the tensile strength value provided by the supplier. On the other hand, the highest inter-road bond strength for PK8655 was 30.8 ± 3.1 MPa and it was obtained in the sample printed with strand width × height of 5.0 × 3.0 mm and table speed of 15 mm/s. This value is ~ 25% of the tensile strength value provided by the supplier. Both maximum inter road bond strengths (PK6246 and PK8655) were obtained with a strand width of 5 mm.

Besides, the speed of the table had an important influence on PK6246 samples, but it varies according to the geometry of the strand. According to figures 5.12 a and b, that is, for strand widths of 4 mm, it could be observed that an increase in the speed of the table improves the inter-road bond strength while keeping other printing parameters constant. However, for strand widths of 5 mm (Figure 5.12 a and b) and 6 mm (Figure 5.12 a and

b) an opposite effect was found, that is, an increase in the speed of the table reduced the inter-road bond strength of the samples. A similar behavior was found in the PK8655 samples, but here the speed of the table had only a positive influence (higher inter-road bond strength) for strand widths of 4.0, 5.0 and 6.0 mm. These behaviors are due to two problems that occur during printing. The first is due to very slow cooling and the excessive accumulation of heat, which can cause deformation and sinking of the printed workpiece. The second is due to very rapid cooling, which can cause a warping effect mainly during the printing of the first strands. Thus, the printed workpieces were analyzed with both speeds to find the optimal parameters.

Furthermore, strand heights had also influence in the inter-road bond strengths. The highest strengths were normally found within the range of strand heights (1.5 mm to 3.5 mm). For instance, the highest inter-road bond strengths in Figure 5.13 (strand width of 4 mm and table speed of 15 mm/s) were 40.7 ± 4.6 MPa (for PK6246) and 20.3 ± 2.5 MPa (for PK8655). However, there are some exceptions as shown in Figure 5.12 a, in which the maximum inter-road bond strength was given with a strand height of 3.5 mm for the PK8655 sample. As with determining the optimal table speed, the problems of slow cooling (heat accumulation) and rapid cooling (warping effect) during printing must be considered to determine the strand geometry that presents the greatest inter-road bond strengths. Bellini et al. (2003) claims lower printing speeds and thinner strand heights generally improve inter-road bond strength by allowing more time for polymer diffusion and reducing void formation. However, very low speeds can lead to excessive heating and material degradation. Thus, depending on the type of material, strand width, and table speed, an optimal strand height can be determined for each situation.

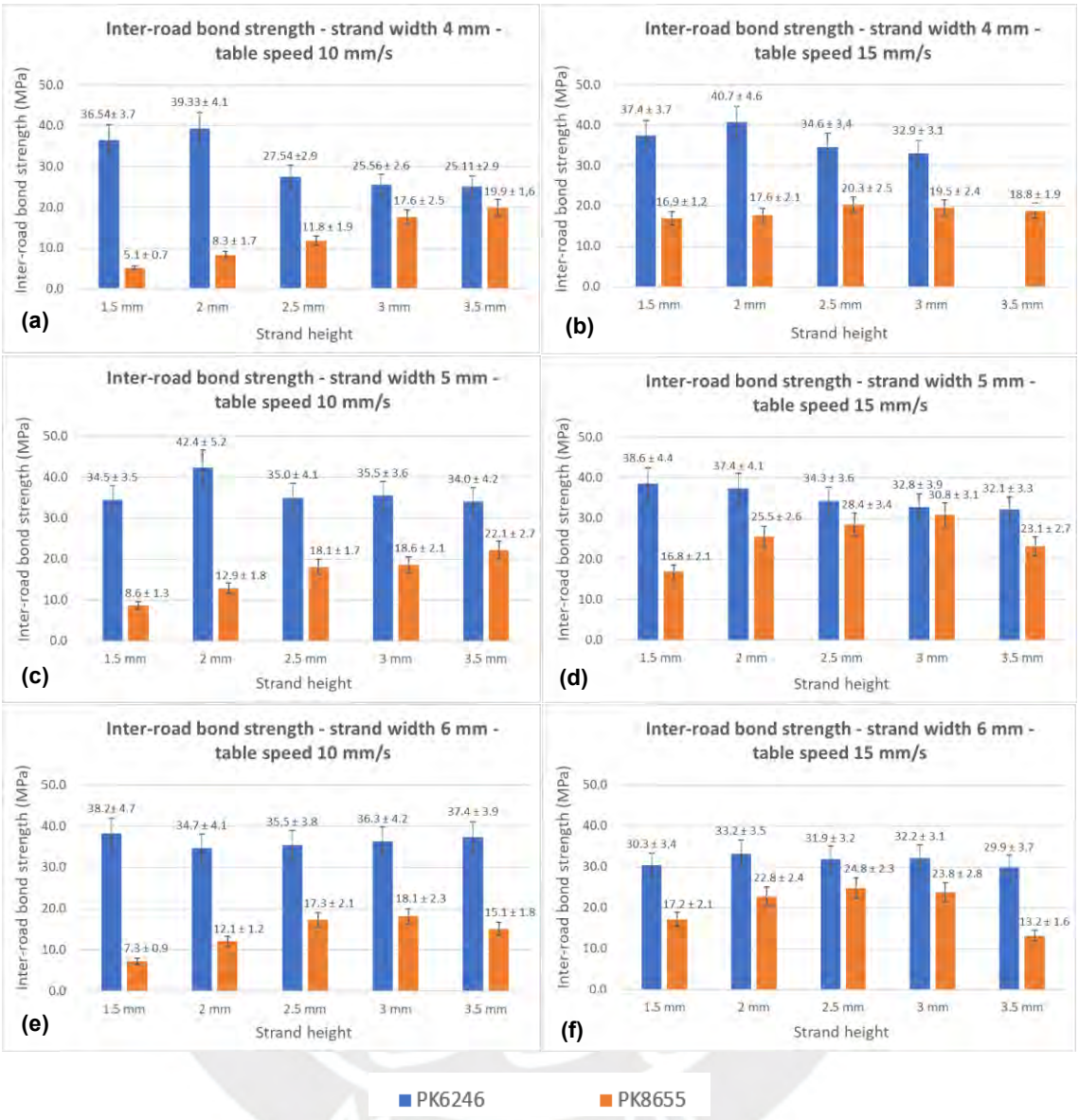

Figure 5.12. Inter-road bond strengths for: (a) strand width 4 mm and table speed 10 mm/s; (b) strand width 4 mm and table speed 15 mm/s; (c) strand width 5 mm and table speed 10 mm/s; (d) strand width 5 mm and table speed 15 mm/s; (e) strand width 6 mm and table speed 10 mm/s; (f) strand width 6 mm and table speed 15 mm/s.

Figures 5.13 shows the diagrams of tensile force vs position for all printed samples (PK6246 and PK8655). A considerable difference in maximum tensile forces could be observed between both types of materials, as was the case with the maximum inter-road bond strengths. For the maximum inter-road bond strength of the PK6246 sample (42.4

± 5.2 MPa), the tensile force was ~4700 N. Likewise, for the maximum inter-road bond strength of PK8655 sample (30.8 ± 3.1 MPa), the tensile force was ~2500 N.

Furthermore, a great difference in elongation could also be observed for the different samples of both materials. This was possibly due to the anisotropic properties of the printed workpieces. Insufficient adhesion between adjacent strands, resulting from incomplete diffusion and neck growth, is a significant factor contributing to material anisotropy, especially mechanical anisotropy (Aliheidari et al., 2018). Another factor contributing to anisotropy is the presence of significant air voids that form between adjacent cylindrical lines during the printing process (Ziemian et al., n.d.). According to Zohdi & Yang et al. (2021), other factors to consider are the build orientation, the thickness of the strand and the thermal conductivity of the material. Likewise, there are some methods to reduce the anisotropy of printed materials such as adding fillers, polymer and monomer alternation, and post-processing heat treatment.

Finally, a greater difference in elongation could be observed between the PK6246 and PK8655 samples. This is due to the existence of glass fibers within the PK8655 samples. Q. Ding et al. (2020) studied the impact of incorporating carbon fiber to mitigate anisotropy in FDM printed components. Orienting the carbon fiber along the printing direction increased the anisotropy of the material and improved directional properties, particularly strength. While adjusting strand thickness and printing temperatures effectively reduced anisotropy in parts printed sideways and crosswise, samples printed in the longitudinal build orientation still showed significant differences compared to those printed in other orientations.

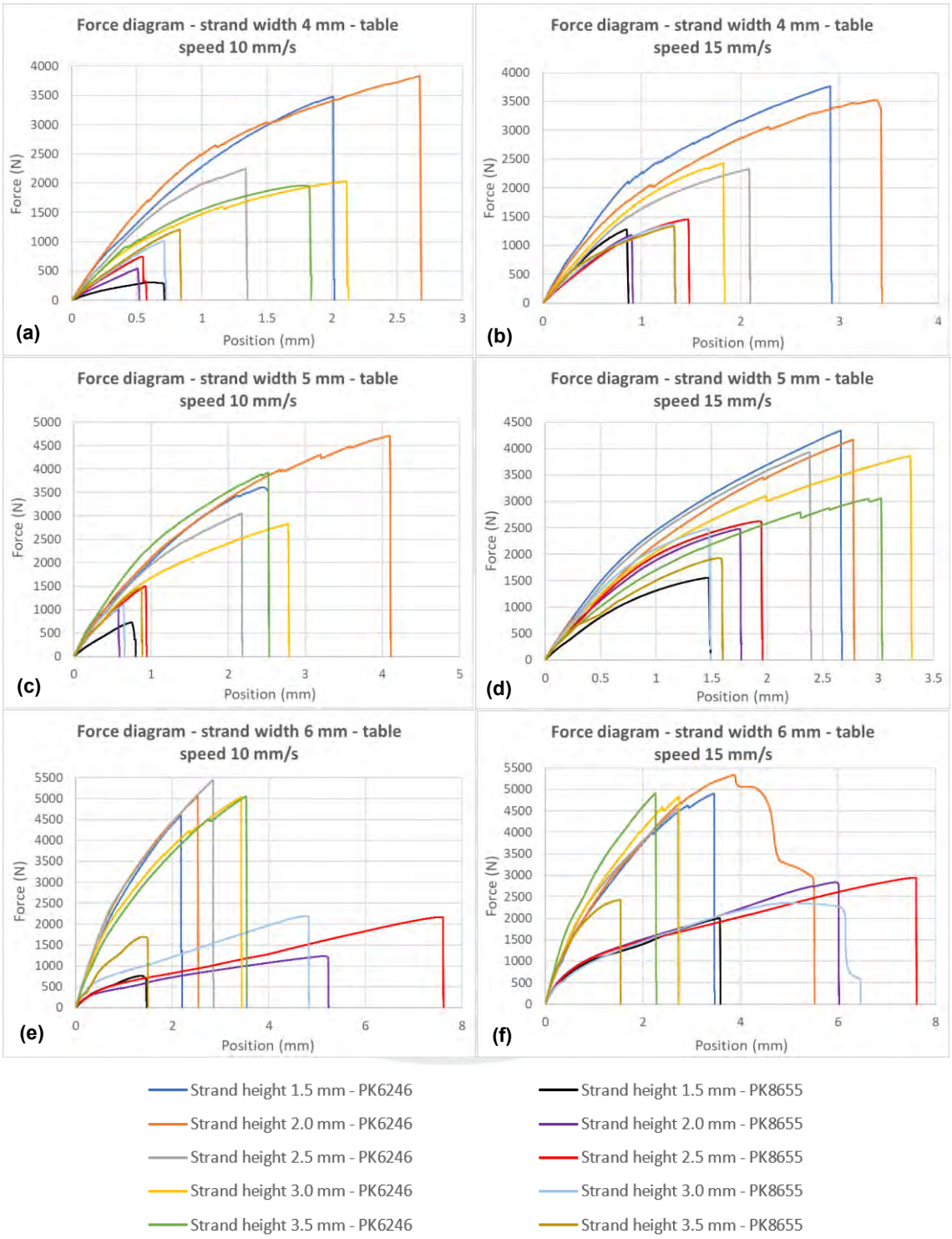

Figure 5.13. Tensile force vs position for: (a) strand width 4 mm and table speed 10 mm/s; (b) strand width 4 mm and table speed 15 mm/s; (c) strand width 5 mm and table speed 10 mm/s; (d) strand width 5 mm and table speed 15 mm/s; (e) strand width 6 mm and table speed 10 mm/s; (f) strand width 6 mm and table speed 15 mm/s.

5.4 Materialography

Figures 5.24, 5.25, 5.26 and 5.27 show cross-section macrographs of the workpieces (PK6246 and PK8655) with strand width of 5 mm and table speeds of 10 and 15 mm/s. These series of parameters were chosen due they showed the highest inter-road bond strengths. Besides, these macrographs were captured in the central section of the samples, which measured approximately 30 mm in length.

It can be seen considerably greater number of pores in the PK8655 samples (Figures 5.26 and 5.27) than in the PK6246 samples (Figures 5.24 and 5.25). Several of these pores were possible due to the presence of glass fibers. Likewise, this large number of pores in the PK8655 samples is related to the low inter-road bond strengths found in section 5.3. For instance, in Figure 5.12 c, the PK8655 sample printed with strand width × height of 5.0 × 2.5 mm and table speed of 10 mm/s had an inter-road bond strength of 18.1 ± 1.7 MPa. Furthermore, some of the pores in the PK8655 samples were possibly tunnels, which further impairs its mechanical properties. On the other hand, some pores were also observed in the PK62646 samples (Figures 5.24 and 5.25). Likewise, it was found that increasing the height of the strands reduces the number of pores. This is due to the influence of cooling between the strands, that is, reducing the cooling speed causes better adhesion between strands and therefore fewer pores.

Another important aspect that could be observed was the different shapes of the strands according to the strand height (from 1.5 to 3.5). As the strand height increased, the waviness of the sample surfaces increased and the inter-road bond lines decreased up to ~40%. These variations in the shapes of the strands definitely affect their mechanical properties (inter-road bond strengths). Although research directly linking waviness to inter-road bond lines varies across studies, the collective findings emphasize the importance of minimizing waviness to enhance bond line quality and overall mechanical performance in additive manufacturing (Nguyen et al., 2024). Thus, to achieve improved mechanical properties, it is essential to use lower strand heights, while ensuring they are not so low that porosity increases.

Finally, some delaminations were observed in the samples (PK6246 and PK8655) with very low strand heights (1.5 mm and 2.0 mm). This was due to rapid cooling (low interpass temperature) and is related to the warping effect explained above. In the PK 6246 sample (Figure 5.24) obtained with strand width x height 5.0 x 1.5 mm and table

speed of 10 mm/s, the delamination occurred as a result of the low interpass temperature (~165 °C), which confirms the assumption from section 3.2. Most affected are the samples obtained with strand width × height 5.0 × 1.5 mm for both materials. Adding compatibilizers, coupling agents, or fillers such as carbon fibers can enhance interstrand bonding. However, the dispersion and interaction of these additives must be carefully managed. Shofner et al. (2003) found that carbon nanotubes improve mechanical properties and reduce delamination but require precise dispersion techniques to avoid agglomeration and ensure uniformity.

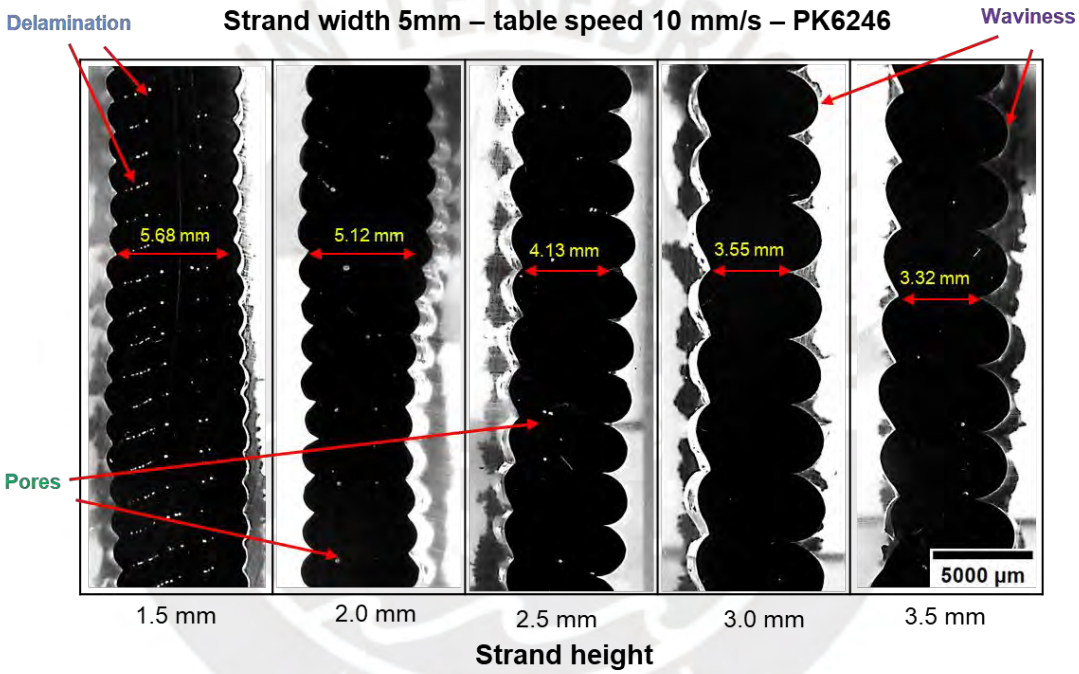

Figure 5.14. Macrographs of PK6246 samples obtained with strand width of 5 mm and table speed of 10 mm/s speed.

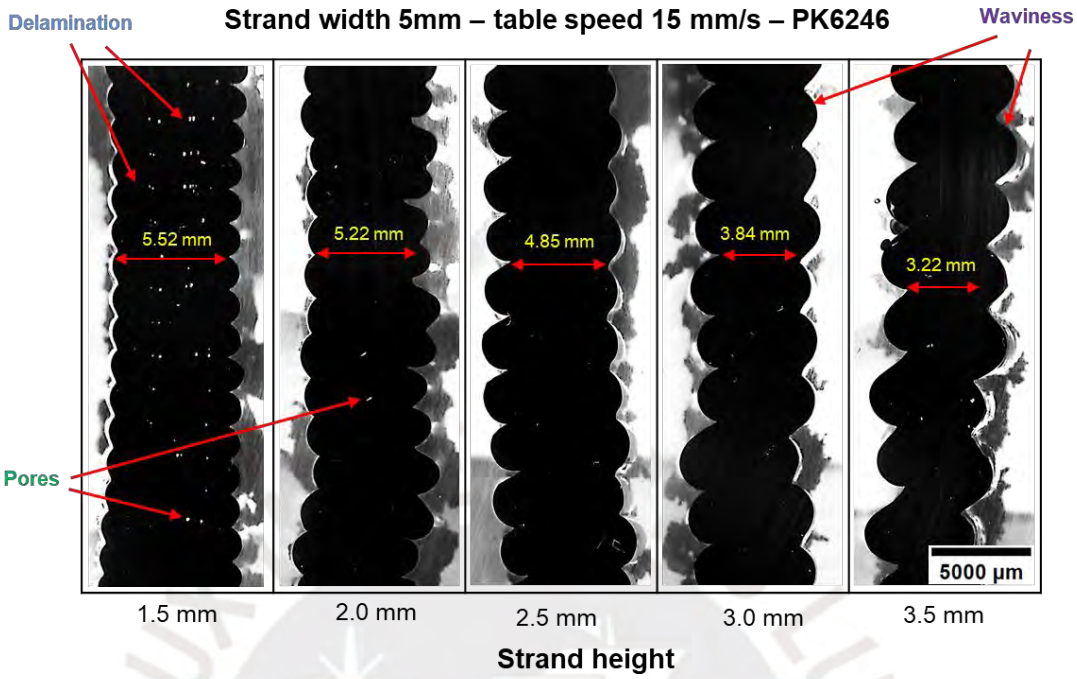

Figure 5.15. Macrographs of PK6246 samples obtained with strand width of 5 mm and table speed of 15 mm/s speed.

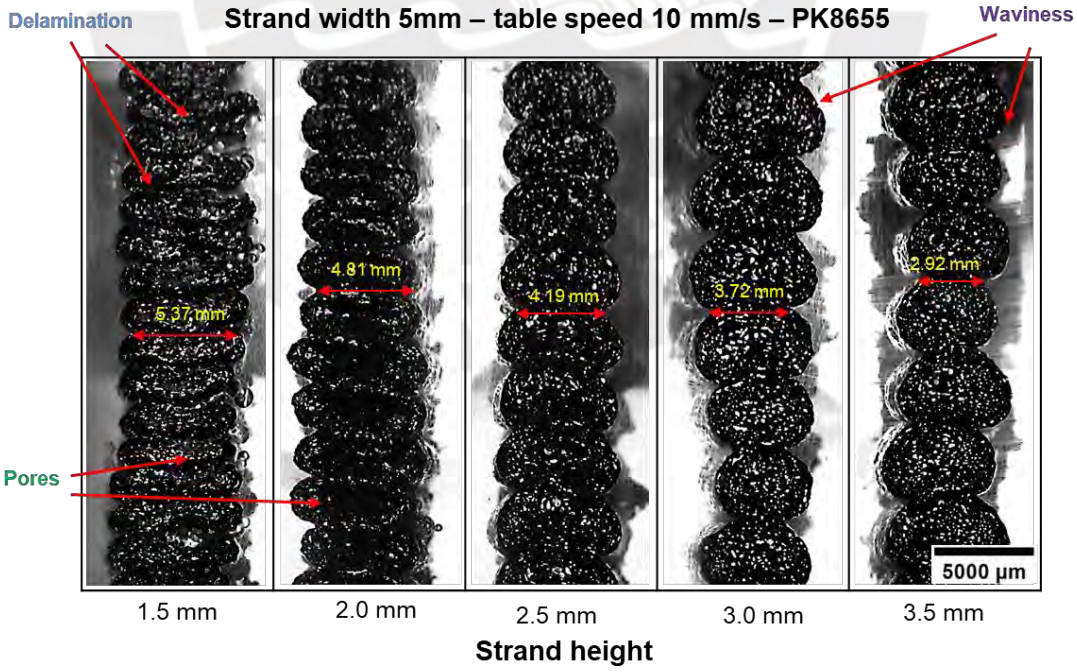

Figure 5.16. Macrographs of PK8655 samples obtained with strand width of 5 mm and table speed of 10 mm/s speed.

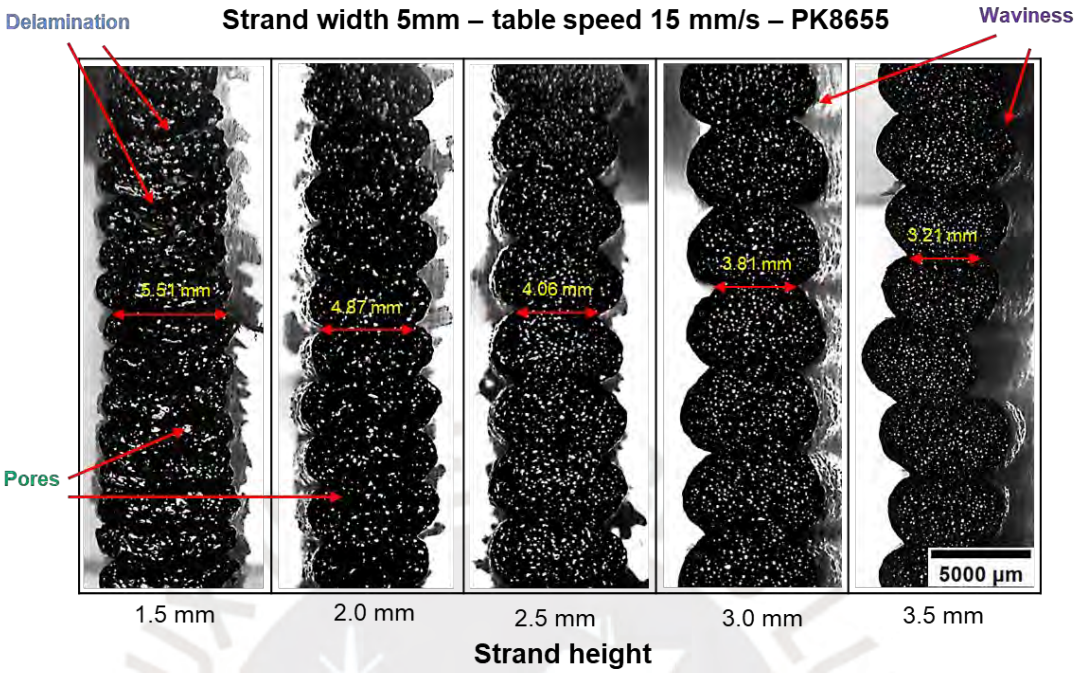

Figure 5.17. Macrographs of PK8655 samples obtained with strand width of 5 mm and table speed of 15 mm/s speed.

5.5 TGA analysis

Figure 5.18 shows the results of TGA analysis for granulates and samples of PK6246 and PK8655 material. The samples with a strand width of 5.0 mm and table speed of 10 mm/s were chosen because they presented the highest inter-road bond strengths (see Section 5.3). Most degradation temperatures were observed above 300 °C. However, during the extrusion process of the workpieces, polyketone degraded below 300 °C. This is because the degradation temperature is time-dependent; in other words, the material can degrade at lower temperatures than the specified degradation temperature if it is exposed for a longer duration. In addition, it was observed that the PK6246 material is more stable than the PK8655 material in its granular form (base material) since it has a higher degradation temperature, that is, a higher temperature is required for the material to degrade.

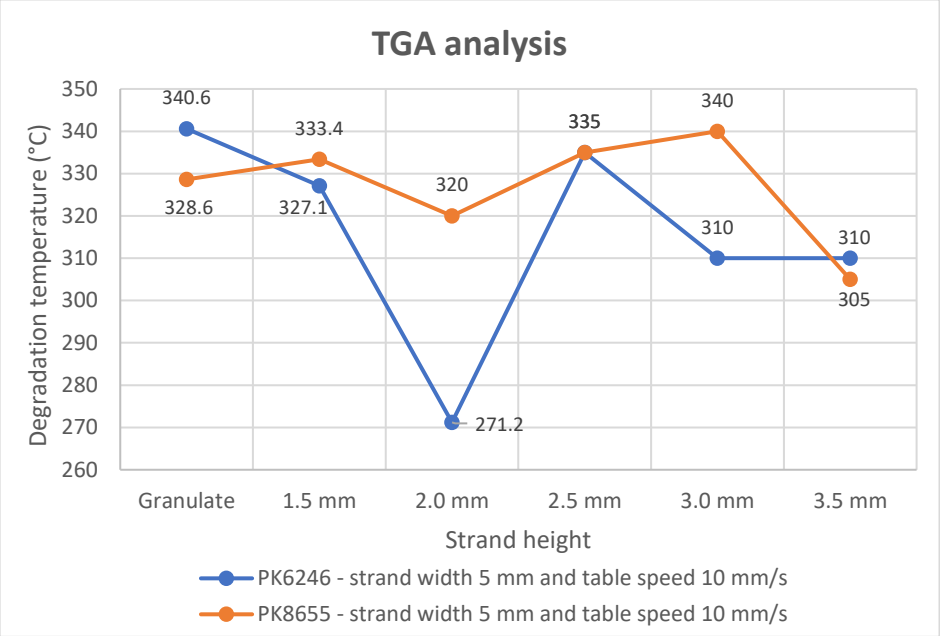

Figure 5.18. Results of TGA analysis for PK6246 and PK8655 materials.

On the other hand, a lower stability was observed in the printed samples of the PK6246 material, with the sample of strand width × height of 5.0 × 2.0 mm and table speed of 10 mm/s having the worst thermal stability with a degradation temperature of 271.2 °C. Likewise, the sample with strand width × height of 5.0 × 3.0 mm and table speed of 10 mm/s presented the greatest thermal stability of the PK8655 material with a degradation temperature of 340 °C.

In general, the PK8655 material presents a slightly more stable behavior than the PK6246 material, possibly due to the presence of glass fibers in its composition. Liu et al. (2021) studied the thermal behavior of glass/polyimide composites under different driving conditions, including radiation. It was employed numerical simulations and sequentially adopted multiscale unit cell models for polyimide (PI), glass fibers and composite materials. A finite element model was developed using triangular and tetrahedral elements to create 2D and 3D meshes, respectively. The findings indicated that the effective thermal conductivity of PI decreases as porosity increases, reaching a maximum reduction of 39.5%. Furthermore, the effective transverse thermal conductivity of glass fiber increases with higher fiber volume fractions, showing a maximum increase of 49.0%.

Conclusions

This thesis work shows that stable workpieces made with PK6246 can be produced through extruder-based additive manufacturing when the correct printing parameters are chosen. In contrast, workpieces made with PK8655 showed unstable performance. Furthermore, this work shows and compares new perspectives on the additive manufacturing of parts manufactured from 2 types of polyketones. The following conclusions were summarized based on the results:

- Several critical parameters must be carefully controlled to achieve consistent mechanical properties and stable printed parts. These include factors such as strand geometry, table speed, rotational extruder speed, nozzle diameter, workpiece diameter, building table temperature, and process temperatures. The results show that the strand geometry and the relative speed between the extruder and the table have the most important influence on the interpass temperatures and therefore on the quality of the workpiece.
- With the increase of the relative speed or the geometry of the strand, the interpass temperatures also increase resulting in improved interstrand adhesion. However, after a certain point it begins to deform (sinking) due to the high accumulation of heat. Likewise, very low relative speed or strand geometry also affects the workpiece geometry caused by warping due to rapid cooling. Therefore, the optimal printing parameters are close to the center of the established range. Although the optimal parameters for the PK6246 and PK8655 pieces are different, the best results were found in both cases for a strand width of 5.0 mm.
- With the increase of the strand height (range from 1.5 to 3.5 mm), the waviness of the sample surfaces increase, delamination lines (at low interpass temperatures) and porosity decrease, and the inter-road bond lines decrease up to ~ 40%. These variations in the shapes of the strands affect their mechanical properties (inter-road bond strengths). Thus, to obtain better mechanical properties, it is necessary to set lower strand heights, ensuring that they are not too low and that a low interpass temperature is not generated.
- The highest inter road bond strength (42.4 ± 5.2 MPa) for PK6246 was found in the sample printed with strand width × height of 5.0 × 2.0 mm and table speed of 10 mm/s, and presented an interpass temperature of ~ 185 °C. Likewise, the

highest inter-road bond strength (30.8 ± 3.1 MPa) for PK8655 was found in the sample printed with strand width × height of 5.0 × 3.0 mm and table speed of 15 mm/s, and presented an interpass temperature of ~ 190 °C. Both samples showed an optimal interpass temperature (neither too high nor too low) which caused them to have the highest inter-road bond strength and therefore the best mechanical properties.

- The low inter-road bond strengths found for the PK8655 samples are due mainly to an abundant porosity found in its cross section. There are some possible reasons such as the presence of glass fibers and delaminations caused by low interpass temperatures.

This work has evaluated the feasibility and successfully characterized 2 different types of polyketone. Despite the promising results, several avenues of future work can be pursued to develop and better understand polyketones. As future work, researching and improving the additive production capabilities with polyketone can continue since it is a material with a great potential.

Bibliography

- Adhana, I., Smaradhana, D. F., Ariawan, D., Raharjo, W. W., & Yusuf, B. (2023). Effect of Screw Rotation Speed on Mechanical Properties and Morphology of Abs/Mcc Composites. *Mekanika: Majalah Ilmiah Mekanika*, *22*(1), 23. https://doi.org/10.20961/mekanika.v22i1.70884

- Agarwala, M. K., Jamalabad, V. R., Langrana, N. A., Safari, A., Whalen, P. J., & Danforth, S. C. (1996). Structural quality of parts processed by fused deposition. *Rapid Prototyping Journal*, *2*(4), 4–19. https://doi.org/10.1108/13552549610732034

- *AKROTEK PK-HM 8 black (6246)*. (n.d.). Retrieved July 1, 2024, from file:///C:/Users/Dell/Downloads/AKROTEK%20PK-HM%208%20black%20(6246).pdf

- *AKROTEK PK-VM GF 30 black (8655)*. (n.d.). Retrieved July 1, 2024, from file:///C:/Users/Dell/Downloads/AKROTEK%20PK-VM%20GF%2030%20black%20(8655).pdf

- Aliheidari, N., Christ, J., Tripuraneni, R., Nadimpalli, S., & Ameli, A. (2018). Interlayer adhesion and fracture resistance of polymers printed through melt extrusion additive manufacturing process. *Materials and Design*, *156*, 351–361. https://doi.org/10.1016/j.matdes.2018.07.001

- Al-Muaikel, N. S. (2011). Friedel-crafts polyketones: Synthesis, characterization and antimicrobial properties of unsaturated polyketones and copolyketones based on difurfurylidene cycloheptanone. *International Journal of Polymer Science*, *2011*. https://doi.org/10.1155/2011/810628

- Alsabri, A., Tahir, F., & Al-Ghamdi, S. G. (2021). Life-cycle assessment of polypropylene production in the gulf cooperation council (Gcc) region. *Polymers*, *13*(21). https://doi.org/10.3390/polym13213793

- Altıparmak, S. C., & Xiao, B. (2021). A market assessment of additive manufacturing potential for the aerospace industry. In *Journal of Manufacturing Processes* (Vol. 68, pp. 728–738). Elsevier Ltd. https://doi.org/10.1016/j.jmapro.2021.05.072

- Altıparmak, S. C., Yardley, V. A., Shi, Z., & Lin, J. (2021). Challenges in additive manufacturing of high-strength aluminium alloys and current developments in hybrid additive manufacturing. In *International Journal of Lightweight Materials and Manufacture* (Vol. 4, Issue 2, pp. 246–261). KeAi Publishing Communications Ltd. https://doi.org/10.1016/j.ijlmm.2020.12.004

- Altıparmak, S. C., Yardley, V. A., Shi, Z., & Lin, J. (2022). Extrusion-based additive manufacturing technologies: State of the art and future perspectives. In *Journal of Manufacturing Processes* (Vol. 83, pp. 607–636). Elsevier Ltd. https://doi.org/10.1016/j.jmapro.2022.09.032

- Ambade, V., Rajurkar, S., Awari, G., Yelamasetti, B., & Shelare, S. (2023). Influence of FDM process parameters on tensile strength of parts printed by PLA material. *International Journal on Interactive Design and Manufacturing*. https://doi.org/10.1007/s12008-023-01490-7

- ASTM. ISO/ASTM 52900:2015. (2015). *Standard Terminology for Additive Manufacturing – General Principles – Terminology*. https://doi.org/10.1520/ISOASTM52900-15

- Bae, W. S., Lee, S., & Kim, B. C. (2014). Effect of shear condition on the thermal stabilization of ethylene-propylene-carbon monoxide terpolymer. *Polymer Degradation and Stability*, *105*(1), 160–165. https://doi.org/10.1016/j.polymdegradstab.2014.04.001

- Baiano, A. (2022). 3D Printed Foods: A Comprehensive Review on Technologies, Nutritional Value, Safety, Consumer Attitude, Regulatory Framework, and Economic and Sustainability Issues. *Food Reviews International*, *38*(5), 986–1016. https://doi.org/10.1080/87559129.2020.1762091

- Bellini, A., & Güçeri, S. (2003). Mechanical characterization of parts fabricated using fused deposition modeling. *Rapid Prototyping Journal*, *9*(4), 252–264. https://doi.org/10.1108/13552540310489631

- Berman, B. (2012). 3-D printing: The new industrial revolution. *Business Horizons*, *55*(2), 155–162. https://doi.org/10.1016/j.bushor.2011.11.003

- Bianchi, I., Mancia, T., Mignanelli, C., & Simoncini, M. (2024). Effect of nozzle wear on mechanical properties of 3D printed carbon fiber-reinforced polymer parts by material extrusion. *International Journal of Advanced Manufacturing Technology*, *130*(9–10), 4699–4712. https://doi.org/10.1007/s00170-024-13035-7

- Bikas, H., Stavropoulos, P., & Chryssolouris, G. (2016). Additive manufacturing methods and modeling approaches: A critical review. *International Journal of Advanced Manufacturing Technology*, *83*(1–4), 389–405. https://doi.org/10.1007/s00170-015-7576-2

- Boschetto, A., & Bottini, L. (2015). Surface improvement of fused deposition modeling parts by barrel finishing. *Rapid Prototyping Journal*, *21*(6), 686–696. https://doi.org/10.1108/RPJ-10-2013-0105

- Brion, D. A. J., Shen, M., & Pattinson, S. W. (2022). Automated recognition and correction of warp deformation in extrusion additive manufacturing. *Additive Manufacturing*, *56*. https://doi.org/10.1016/j.addma.2022.102838

- Chacón, J. M., Caminero, M. A., García-Plaza, E., & Núñez, P. J. (2017). Additive manufacturing of PLA structures using fused deposition modelling: Effect of process parameters on mechanical properties and their optimal selection. *Materials and Design*, *124*, 143–157. https://doi.org/10.1016/j.matdes.2017.03.065

- Cho, J., Lee, S. K., Eem, S. H., Jang, J. G., & Yang, B. (2019). Enhanced mechanical and thermal properties of carbon fiber-reinforced thermoplastic polyketone composites. *Composites Part A: Applied Science and Manufacturing*, *126*. https://doi.org/10.1016/j.compositesa.2019.105599

- C.K. Chua, K. F. L. (2014). *3D printing and additive manufacturing: principles and applications (with companion media pack) of rapid prototyping fourth edition*. https://books.google.de/books/about/3d_Printing_And_Additive_Manufacturing_P.html?id=Gy88DQAAQBAJ&redir_esc=y

- Colon, A. R., Kazmer, D. O., Peterson, A. M., & Seppala, J. E. (2023). Characterization of die-swell in thermoplastic material extrusion. *Additive Manufacturing*, *73*. https://doi.org/10.1016/j.addma.2023.103700

- Czyżewski, P., Marciniak, D., Nowinka, B., Borowiak, M., & Bieliński, M. (2022). Influence of Extruder's Nozzle Diameter on the Improvement of Functional Properties of 3D-Printed PLA Products. *Polymers*, *14*(2). https://doi.org/10.3390/polym14020356

- Daminabo, S. C., Goel, S., Grammatikos, S. A., Nezhad, H. Y., & Thakur, V. K. (2020). Fused deposition modeling-based additive manufacturing (3D printing): techniques for polymer material systems. In *Materials Today Chemistry* (Vol. 16). Elsevier Ltd. https://doi.org/10.1016/j.mtchem.2020.100248

- Ding, Q., Li, X., Zhang, D., Zhao, G., & Sun, Z. (2020). Anisotropy of poly(lactic acid)/carbon fiber composites prepared by fused deposition modeling. *Journal of Applied Polymer Science*, *137*(23). https://doi.org/10.1002/app.48786

- Ding, S., Zou, B., Wang, P., & Ding, H. (2019). Effects of nozzle temperature and building orientation on mechanical properties and microstructure of PEEK and PEI printed by 3D-FDM. *Polymer Testing*, *78*. https://doi.org/10.1016/j.polymertesting.2019.105948

- Faidallah, R. F., Hanon, M. M., Szakál, Z., & Oldal, I. (2024). Mechanical characterization of 3D-Printed carbon fiber-reinforced polymer composites and pure polymers: Tensile and compressive behavior analysis. *International Review of Applied Sciences and Engineering*. https://doi.org/10.1556/1848.2024.00796

- Feit S, M. C. (2019). *Climate change: not green, but greenhouse*. https://www.boell.de/en/2019/11/04/climate-change-not-green-greenhouse

- Ford, S., & Despeisse, M. (2016). Additive manufacturing and sustainability: an exploratory study of the advantages and challenges. *Journal of Cleaner Production*, *137*, 1573–1587. https://doi.org/10.1016/j.jclepro.2016.04.150

- Frieden Templeton, W., Hinnebusch, S., Strayer, S. T., To, A. C., Pistorius, P. C., & Narra, S. P. (2024). A mechanistic explanation of shrinkage porosity in laser powder bed fusion additive manufacturing. *Acta Materialia*, *266*. https://doi.org/10.1016/j.actamat.2023.119632

- Gao, W., Zhang, Y., Ramanujan, D., Ramani, K., Chen, Y., Williams, C. B., Wang, C. C. L., Shin, Y. C., Zhang, S., & Zavattieri, P. D. (2015). The status, challenges, and future of additive manufacturing in engineering. *CAD Computer Aided Design*, *69*, 65–89. https://doi.org/10.1016/j.cad.2015.04.001

- George ER. (1989). *Mica and glass reinforced polyketone polymers*.

- George ER. (1992). *Polyketone blend having improved mechanical properties*.

- George Wypych. (2016). *Handbook of Fillers* (Fourth Edition).

- Gergen WP and Machado JM. (1990). *Polyketone polymer blends*.

- Gergen WP, M. J. W. D. and G. RP. (1991). *Blends of linear alternating polyketones, polyamides and olefin-carboxylic acid copolymers*.

- Gibson, I., Rosen, D., Stucker, B., & Khorasani, M. (2021). *Additive Manufacturing Technologies* (3rd ed.). Springer International Publishing. https://doi.org/10.1007/978-3-030-56127-7

- Golhin, A. P., Tonello, R., Frisvad, J. R., Grammatikos, S., & Strandlie, A. (2023). Surface roughness of as-printed polymers: a comprehensive review. In *International Journal of Advanced Manufacturing Technology* (Vol. 127, Issues 3–4, pp. 987–1043). Springer Science and Business Media Deutschland GmbH. https://doi.org/10.1007/s00170-023-11566-z

- Gonzalez-Gutierrez, J., Cano, S., Schuschnigg, S., Kukla, C., Sapkota, J., & Holzer, C. (2018). Additive manufacturing of metallic and ceramic components by the material extrusion of highly-filled polymers: A review and future perspectives. In *Materials* (Vol. 11, Issue 5). MDPI AG. https://doi.org/10.3390/ma11050840

- Gu, X., Wang, Z., Wang, H., Zhou, G., & Zhou, Y. (2021). Synthesis of thermally robust benzimidazolone-based wholly aromatic polyketones. *RSC Advances*, *11*(10), 5444–5450. https://doi.org/10.1039/d0ra09831k

- Gulf Petrochemicals &Chemicals Association. (2016). *GCC Plastic Industry Indicators 2016*. https://gpca.org.ae/wp-content/uploads/2018/03/GCC-Plastics-Industry-Indicators-2016.pdf

- He, Q., Jiang, J., Yang, X., Zhang, L., Zhou, Z., Zhong, Y., & Shen, Z. (2021). Additive manufacturing of dense zirconia ceramics by fused deposition modeling via screw extrusion. *Journal of the European Ceramic Society*, *41*(1), 1033–1040. https://doi.org/10.1016/j.jeurceramsoc.2020.09.018

- Herderick, E. D. (2016). Additive Manufacturing in the Minerals, Metals, and Materials Community: Past, Present, and Exciting Future. In *JOM* (Vol. 68, Issue 3, pp. 721–723). Minerals, Metals and Materials Society. https://doi.org/10.1007/s11837-015-1799-4

- Jeon, H., Park, J., Kim, S., Park, K., & Yoon, C. (2020). Effect of nozzle temperature on the emission rate of ultrafine particles during 3D printing. *Indoor Air*, *30*(2), 306–314. https://doi.org/10.1111/ina.12624

- Joseph Rey, J. R. H., Chen, Q., Maalihan, R. D., Ren, J., da Silva, Í. G. M., Dugos, N. P., Caldona, E. B., & Advincula, R. C. (2021). 3D printing of biomedically relevant polymer materials and biocompatibility. *MRS Communications*, *11*(2), 197–212. https://doi.org/10.1557/s43579-021-00038-8

- Joshi, S. C., & Sheikh, A. A. (2015). 3D printing in aerospace and its long-term sustainability. *Virtual and Physical Prototyping*, *10*(4), 175–185. https://doi.org/10.1080/17452759.2015.1111519

- Jung, Y. S., Canlier, A., & Hwang, T. S. (2018). An efficient and facile method of grafting Allyl groups to chemically resistant polyketone membranes. *Polymer*, *141*, 102–108. https://doi.org/10.1016/j.polymer.2018.03.007

- Kamaal, M., Anas, M., Rastogi, H., Bhardwaj, N., & Rahaman, A. (2021). Effect of FDM process parameters on mechanical properties of 3D-printed carbon fibre–PLA composite. *Progress in Additive Manufacturing*, *6*(1), 63–69. https://doi.org/10.1007/s40964-020-00145-3

- Labus Zlatanovic, D., Hildebrand, J., & Bergmann, J. P. (2023). The study of screw extrusion-based additive manufacturing of eco-friendly aliphatic polyketone. *Journal of Materials Research and Technology*, *25*, 4125–4138. https://doi.org/10.1016/j.jmrt.2023.06.223

- Lagaron, J. M., Vickers, M. E., Powell, A. K., & Davidson, N. S. (n.d.). *Crystalline structure in aliphatic polyketones*.

- Li, G., Lyu, S., Zheng, R., Li, Q., Ameyama, K., Xiao, W., & Ma, C. (2019). Strengthening 2024Al alloy by novel core-shell structured Ti/B4C composite particles. *Materials Science and Engineering: A*, *755*, 231–234. https://doi.org/10.1016/j.msea.2019.04.021

- Liang, J. Z. (2008). Effects of extrusion conditions on die-swell behavior of polypropylene/diatomite composite melts. *Polymer Testing*, *27*(8), 936–940. https://doi.org/10.1016/j.polymertesting.2008.08.001

- Ligon, S. C., Liska, R., Stampfl, J., Gurr, M., & Mülhaupt, R. (2017). Polymers for 3D Printing and Customized Additive Manufacturing. In *Chemical Reviews* (Vol. 117, Issue 15, pp. 10212–10290). American Chemical Society. https://doi.org/10.1021/acs.chemrev.7b00074

- Lim, M. Y., Oh, J., Kim, H. J., Kim, K. Y., Lee, S. S., & Lee, J. C. (2015). Effect of antioxidant grafted graphene oxides on the mechanical and thermal properties of polyketone composites. *European Polymer Journal*, *69*, 156–167. https://doi.org/10.1016/j.eurpolymj.2015.06.009

- Lin, H., Pearson, A., Kazemi, Y., Kakroodi, A., Hammami, A., Heydrich, M., Xu, B., & Naguib, H. E. (2020). Influence of hygrothermal conditioning on the chemical structure and thermal mechanical properties of aliphatic polyketone. *Polymer Degradation and Stability*, *179*. https://doi.org/10.1016/j.polymdegradstab.2020.109260

- Liu, M., Chen, B., Zhang, D., Wang, Y., & Kan, P. (2021). Numerical studies on effective thermal conductivities of the glass/polyimide composite materials under the conditions of conduction & radiation. *International Journal of Heat and Mass Transfer*, *180*. https://doi.org/10.1016/j.ijheatmasstransfer.2021.121764

- Marklund, E., Gedde, U., Hedenqvist, M., & Wiberg, G. (n.d.). *Properties of polyketone/polypropylene blends*. www.elsevier.nl/locate/polymer

- Matsumoto, K., Fukui, C., Shoji, R., & Jikei, M. (2020). Synthesis of aromatic polyketones by nonstoichiometric Friedel-Crafts polycondensation using AlCl3. *Polymer Chemistry*, *11*(26), 4221–4227. https://doi.org/10.1039/d0py00534g

- Melton, G. H., Peters, E. N., & Arisman, R. K. (n.d.). *2 Engineering Thermoplastics*.

- Mi HL, L. D. B. H. K. B. K. M. M. S. (2016). *Polym Korea*. *40*, 225–231.

- Mohd Pu'ad, N. A. S., Abdul Haq, R. H., Mohd Noh, H., Abdullah, H. Z., Idris, M. I., & Lee, T. C. (2019). Review on the fabrication of fused deposition modelling (FDM) composite filament for biomedical applications. *Materials Today: Proceedings*, *29*, 228–232. https://doi.org/10.1016/j.matpr.2020.05.535

- Mousapour, M., Salmi, M., Klemettinen, L., & Partanen, J. (2021). Feasibility study of producing multi-metal parts by Fused Filament Fabrication (FFF) technique. *Journal of Manufacturing Processes*, *67*, 438–446. https://doi.org/10.1016/j.jmapro.2021.05.021

- Nguyen, K. Q., Vuillaume, P. Y., Hu, L., Vachon, A., Diouf-Lewis, A., Marcoux, P. L., Robert, M., & Elkoun, S. (2024). Effect of in situ thermal treatment on interlayer adhesion of 3D printed polyetherimide (PEI) parts produced by fused deposition modeling (FDM). *Materials Today Communications*, *39*. https://doi.org/10.1016/j.mtcomm.2024.108588

- Nurhudan, A. I., Supriadi, S., Whulanza, Y., & Saragih, A. S. (2021). Additive manufacturing of metallic based on extrusion process: A review. In *Journal of Manufacturing Processes* (Vol. 66, pp. 228–237). Elsevier Ltd. https://doi.org/10.1016/j.jmapro.2021.04.018

- Olsson, A., Hellsing, M. S., & Rennie, A. R. (2017). New possibilities using additive manufacturing with materials that are difficult to process and with complex structures. In *Physica Scripta* (Vol. 92, Issue 5). Institute of Physics Publishing. https://doi.org/10.1088/1402-4896/aa694e

- Petrovic, V., Vicente Haro Gonzalez, J., Jordá Ferrando, O., Delgado Gordillo, J., Ramón Blasco Puchades, J., & Portolés Griñan, L. (2011). Additive layered manufacturing: sectors of industrial application shown through case studies.

International Journal of Production Research, *49*(4), 1061–1079. https://doi.org/10.1080/00207540903479786

- Sames, W. J., List, F. A., Pannala, S., Dehoff, R. R., & Babu, S. S. (2016). The metallurgy and processing science of metal additive manufacturing. In *International Materials Reviews* (Vol. 61, Issue 5, pp. 315–360). Taylor and Francis Ltd. https://doi.org/10.1080/09506608.2015.1116649

- Schmidt, L., Schricker, K., Bergmann, J. P., Hussenöder, F., & Eiber, M. (2019). Characterization of a granulate-based strand deposition process in the FLM-method for definition of material-dependent process strategies. *Rapid Prototyping Journal*, *25*(1), 104–116. https://doi.org/10.1108/RPJ-09-2017-0186

- Shofner, M. L., Lozano, K., Rodríguez-Macías, F. J., & Barrera, E. V. (2003). Nanofiber-reinforced polymers prepared by fused deposition modeling. *Journal of Applied Polymer Science*, *89*(11), 3081–3090. https://doi.org/10.1002/app.12496

- Smith, Z. J., Golias, C. J., Vaske, T. J., Young, S. A., Chen, Q., Goodbred, L., Rong, L., Cheng, X., Penumadu, D., & Advincula, R. C. (2024). Correlating viscosity and die swell in 3D printing of polyphenylsulfone: A thermo-mechanical optimization modus operandi. *Reactive and Functional Polymers*, *194*. https://doi.org/10.1016/j.reactfunctpolym.2023.105795

- Spoerk, M., Gonzalez-Gutierrez, J., Sapkota, J., Schuschnigg, S., & Holzer, C. (2018). Effect of the printing bed temperature on the adhesion of parts produced by fused filament fabrication. *Plastics, Rubber and Composites*, *47*(1), 17–24. https://doi.org/10.1080/14658011.2017.1399531

- Stadlbauer, M., Eder, G., & Janeschitz-Kriegl, H. (n.d.). *Crystallization kinetics of two aliphatic polyketones*. www.elsevier.nl/locate/polymer

- Stavropoulos, P., Foteinopoulos, P., Papacharalampopoulos, A., & Tsoukantas, G. (2019). Warping in SLM additive manufacturing processes: estimation through thermo-mechanical analysis. *International Journal of Advanced Manufacturing Technology*, *104*(1–4), 1571–1580. https://doi.org/10.1007/s00170-019-04105-2

- Tang, F., & Jeong, Y. G. (2023). Enhancement in thermal stability and mechanical performance of modified polyketone/aramid short fiber composites with controlled interface. *Composites Part A: Applied Science and Manufacturing*, *171*. https://doi.org/10.1016/j.compositesa.2023.107558

- Thesiya, D., & Lepsik, P. (2023). *An Effective Development of Residual Stresses in Fused Deposit Modelling (FDM): An Overview* (pp. 245–258). https://doi.org/10.2991/978-94-6463-182-1_26

- Tseng, J. W., Liu, C. Y., Yen, Y. K., Belkner, J., Bremicker, T., Liu, B. H., Sun, T. J., & Wang, A. B. (2018). Screw extrusion-based additive manufacturing of PEEK. *Materials and Design*, *140*, 209–221. https://doi.org/10.1016/j.matdes.2017.11.032

- Uriondo, A., Esperon-Miguez, M., & Perinpanayagam, S. (2015). The present and future of additive manufacturing in the aerospace sector: A review of important aspects. In *Proceedings of the Institution of Mechanical Engineers, Part G: Journal of Aerospace Engineering* (Vol. 229, Issue 11, pp. 2132–2147). SAGE Publications Ltd. https://doi.org/10.1177/0954410014568797

- Wang, H., Desilles, N., Follain, N., Marais, S., & Burel, F. (2016). Dimethylketene-based aliphatic polyketones: Copolymers and star-shaped polymers potentially useful in food packaging. *European Polymer Journal*, *85*, 411–420. https://doi.org/10.1016/j.eurpolymj.2016.10.044

- Xu, C., Long, X., He, Y., Fang, X., Huang, K., & Huang, J. (2022). Optimization of the Metal Nozzle for High-Temperature Extrusion Additive Manufacturing. In *Key Engineering Materials* (Vol. 922, pp. 129–136). Trans Tech Publications Ltd. https://doi.org/10.4028/p-tajbmc

- Yadav, P., Dev, S., Hussain, I., & Kumar, R. (2022). Evaluation of additive manufacturing process parameters for improved mechanical properties of thermoplastic parts. *Materials Today: Proceedings*. https://doi.org/10.1016/j.matpr.2022.12.150

- Yang, Y., Li, S. Y., Bao, R. Y., Liu, Z. Y., Yang, M. B., Tan, C. Bin, & Yang, W. (2018). Progress in polyketone materials: blends and composites. In *Polymer International*

(Vol. 67, Issue 11, pp. 1478–1487). John Wiley and Sons Ltd. https://doi.org/10.1002/pi.5624

- Yao, T., Ye, J., Deng, Z., Zhang, K., Ma, Y., & Ouyang, H. (2020). Tensile failure strength and separation angle of FDM 3D printing PLA material: Experimental and theoretical analyses. *Composites Part B: Engineering*, *188*. https://doi.org/10.1016/j.compositesb.2020.107894

- Yonezawa, N., & Okamoto, A. (2009). Synthesis of wholly aromatic polyketones. In *Polymer Journal* (Vol. 41, Issue 11, pp. 899–928). https://doi.org/10.1295/polymj.PJ2007210

- Ziemian, C., Sharma, M., & Ziemian, S. (n.d.). *7 Anisotropic Mechanical Properties of ABS Parts Fabricated by Fused Deposition Modelling*. www.intechopen.com

- Zohdi, N., & Yang, R. C. (2021). Material anisotropy in additively manufactured polymers and polymer composites: A review. In *Polymers* (Vol. 13, Issue 19). MDPI. https://doi.org/10.3390/polym13193368

- Zuiderduin, W. C. J., Homminga, D. S., Huétink, H. J., & Gaymans, R. J. (2003). Influence of molecular weight on the fracture properties of aliphatic polyketone terpolymers. *Polymer*, *44*(20), 6361–6370. https://doi.org/10.1016/S0032-3861(03)00635-9

- Zuiderduin, W. C. J., Homminga, D. S., Huétink, J., & Gaymans, R. J. (2005). Influence of copolymerisation on fracture behaviour of aliphatic polyketones. *Polymer*, *46*(6), 1921–1934. https://doi.org/10.1016/j.polymer.2004.12.032

- Zuiderduin, W. C. J., Huétink, J., & Gaymans, R. J. (2006). Rigid particle toughening of aliphatic polyketone. *Polymer*, *47*(16), 5880–5887. https://doi.org/10.1016/j.polymer.2006.05.077